Tailoring Supramolecular Assemblies on a Metal Surface by Specifically Functionalized Porphyrins

Inauguraldissertation

zur

Erlangung der Würde eines Doktors der Philosophie

vorgelegt der

Philosophisch-Naturwissenschaftlichen Fakultät

der Universität Basel

von

Nikolai Wintjes

aus Marl (NRW, Deutschland)

Basel, 2007

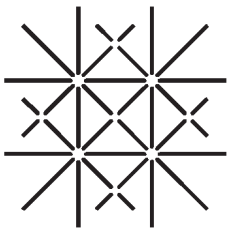

Genehmigt von der Philosophisch-Naturwissenschaftlichen Fakultät auf Antrag von

Prof. Dr. H.-J. Güntherodt
Dr. T. A. Jung
PD Dr. H. Spillmann

Basel, den 29.10.07

Prof. Dr. Hans-Peter Hauri, Dekan

Iam provideo animo, velut qui proximis litori vadis inducti mare pedibus ingrediuntur, quidquid progredior, in vastiorem me altitudinem ac velut profundum invehi et crescere paene opus, quod prima (quaeque perficiendo) minui videbatur.

Livius 31,5

Abstract

The self-assembly behavior of porphyrin derivatives bearing different substituents is investigated on metal surfaces by Scanning Tunneling Microscopy (STM). Different methods to control the self-assembly process by skillful changes of the molecular substituents are developed. It is shown how one-dimensional wires as well as two-dimensional nanoporous networks can be formed by the same molecular compound depending on the coverage. The nanoporous networks can be altered in their pore characteristics and pore-to-pore distances in a controlled way. This is exploited to form a fully self-assembled supramolecular device. The characteristics of the device are studied in detail and it is shown that it can be operated by the tip of an STM. Finally, bimolecular systems are investigated. Here it is shown how the need to balance losses of entropy which is a common factor in all self-assembled networks, can be exploited to direct the self-assembly of such systems to form either separated phases or an intermixed network.

Contents

List of Figures

Abbreviations

DRAM	Dynamic Random Access Memory
DOS	Density Of States
ETH	Eidgenössische Technische Hochschule
LDOS	Local Density Of States
HOMO	Highest Occupied Molecular Orbital
LUMO	Lowest Unoccupied Molecular Orbital
MO	Molecular Orbital
ML	Monolayer
STM	Scanning Tunneling Microscopy or Scanning Tunneling Microscope
UHV	Ultra High Vacuum
P1 - P4	Porphyrin derivative 1 to 4
ZnOEP	zinc-octaethyl porphyrin

Chapter 1

Introduction

For many decades, miniaturization has been one of the main driving forces in scientific and economic progress. In the year 2003, lithographical miniaturization, as measured by the *DRAM half pitch*[1] has reached the 100 nm mark and is supposed to continue shrinking[2].

But with the decreasing feature size new problems are arising. The stability of the smaller structures is decreasing. Going hand in hand with this, the amount of defective structures rises. Another main problem of nowadays electronical devices, emerging from the increased power density, is their high power consumption and heat dissipation.

Therefore, there is a vast interest in finding new approaches to miniaturization that can overcome the aforementioned problems. One of these approaches takes advantage of an effect well-known from biology: the self-assembling capability of organic molecules. While nowadays devices and circuits are built by the so-called "top-down" approach (which means that structures are created out of bigger building blocks, e.g. by lithographic structuring), organic molecules can assemble on technological relevant surfaces, e.g. metal surfaces, without further need of manual construction into highly complex structures, driven only by intermolecular binding forces ("bottom-up" approach). Here, each molecule serves as a unique building block that can be functionalized by chemical synthesis, which makes it possible to control the properties of the eventually assembled structures. Because organic molecules are about a factor of 20 smaller than the smallest structures fabricated nowadays by the "top-down" approach, and because they can be pro-

[1] The *DRAM half pitch* is the average of half the distance between two metal lines connecting the cells of a DRAM memory device. The factor 1/2 takes care of the fact, that the distance also includes the free space between the lines.

[2] http://www.itrs.net/Links/2004Update/2004_01_Design.pdf, http://www.itrs.net/Links/2006Update/FinalToPost/02_Design_2006Update.pdf

duced in vast amounts with only a small number of defects and sometimes even self-healing capabilities, the "bottom-up" approach is widely believed to be the next step in the miniaturization process.

However, there is still a lot of knowledge to be gathered in order to fully control the self-assembling process. Although in solution and the bulk state chemists have developed highly sophisticated methods, it turns out that it is difficult to transfer these principles to surfaces, where the motional degree of freedom is limited to two dimensions and interactions with the substrate influence the system. Therefore, a good understanding of the self-assembly process on surfaces is a key for building technologically relevant, functional devices via the "bottom-up" approach.

In this thesis, different principles to control the self-assembly behavior of porphyrin derivatives are studied. The results are presented in section 3, after in section 2 a brief introduction into the applied methods and materials is presented. In section 3.1 it will be shown that with the same molecular building block either one-dimensional wires or two-dimensional nanoporous networks can be formed on the same substrate depending on the molecular coverage. By subtle changes of the molecular architecture, furthermore the pore-to-pore distance inside these networks will be altered. In section 3.2 such a nanoporous network will be used as the basis for a fully self-assembled supramolecular device. The characteristics of the device, especially its behavior at different temperatures and the activation energy for rotation, will be studied in detail. It will be shown that an individual device can be adressed and operated by the tip of a Scanning Tunneling Microscope (STM). Finally, in section 3.3 bimolecular systems are investigated. Here it will be shown how the balance between entropy and enthalpy can be used to form intermixed networks. These types of network are widely believed to be a key to the understanding of the self-assembly process.

Chapter 2

Methods and Materials

2.1 Scanning Tunneling Microscopy

Invented in 1981 by Gerd Binnig and Heinrich Rohrer at the IBM Zürich Research Laboratory,[1, 2] the Scanning Tunneling Microscope (STM, which is also the abbreviation for scanning tunneling microscopy) has become a powerful tool for studies at the nanoscale. STM is a real-space method, which circumvents the rather complicated interpretations of experiments in the reciprocal space. Because of its high resolution, even single atoms can be made visible[3]. Furthermore, STM experiments yield information about the local characteristics of the probed sample and do not provide mean values over rather large areas. Next to its imaging power, the STM bears spectroscopical capabilities and even allows for the manipulation of single atoms or molecules. Therefore, the STM has been the techinque of choice for this thesis. However, as the STM is based on the quantum mechanical tunneling effect, it needs a conductive or semi-conductive surface as a substrate for the investigated samples.

2.1.1 Basic Theory

The STM consists mainly of a sharp metallic tip (preferentially with a monoatomic apex) which is brought into close proximity (typically a few Å) of a (semi-) conductive surface. Based on the quantum mechanical tunneling effect, electrons can tunnel through the gap between tip and sample. By applying a small bias voltage (usually in the range of 0.01 to 3 V) a directed tunneling current occurs, which is highly depending on the distance

[3] Although there are hints that the resolution of the Atomic Force Microscope is even better and subatomic resolution can be achieved with it.[3]

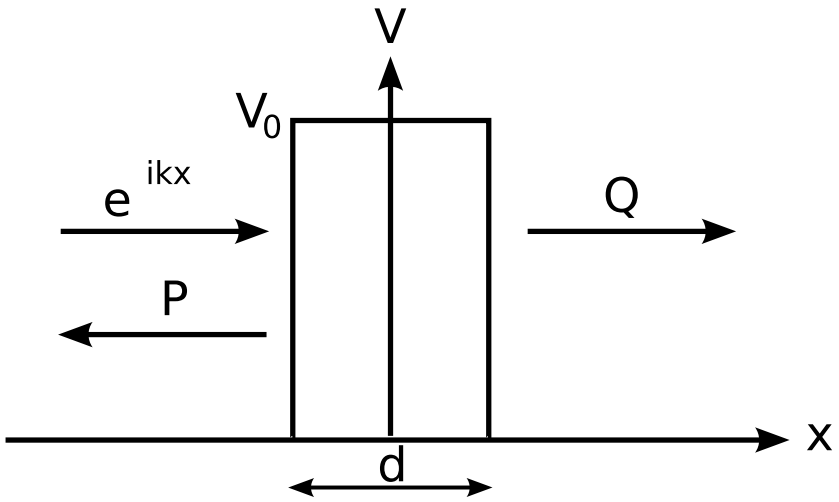

Figure 2.1: One-dimensional model for the quantum mechanical tunneling effect. A (partical) wave (e^{ikx}, coming from the left) faces a potential V_0 that is larger than the energy of the wave. In the classical case the wave is completely reflected by the potential: The propabilities to find the wave on either side of the potential are $P = 1, Q = 0$. Quantum mechanically the propability Q to detect the wave on the right side of the potential can be > 0.

between tip and sample. Therefore, while the tip scans over the sample surface by means of piezo-electric actuators (x- and y-piezos) to obtain a two-dimensional map, even small corrugations lead to changes in the measured tunneling current. By another piezo-electric element (the z-piezo) the height of the tip above the sample can be varied.

Several different scanning modes are possible. In the *constant height* mode, the tip scans over the sample with the z-piezo held at a constant value while the current is being measured as reference signal. Alternatively, in the *constant current* mode a feedback system is used to keep the tunneling current constant. This is achieved by adjusting the tip-sample distance via the z-piezo. The changes in the z-direction are then taken as the reference signal. The latter mode also provides the possibility to scan over surfaces that are not perfectly horizontally aligned, but has the disadvantage of lower scanning speed. The *constant current* mode was used for all images taken in this thesis. To visualize the STM image, the recorded reference signal is depicted at every point of the two dimensional map by a pre-defined color code. In this thesis, the color code for each image was chosen in a way that darker colors reflect less height on the sample. However it has to be noted

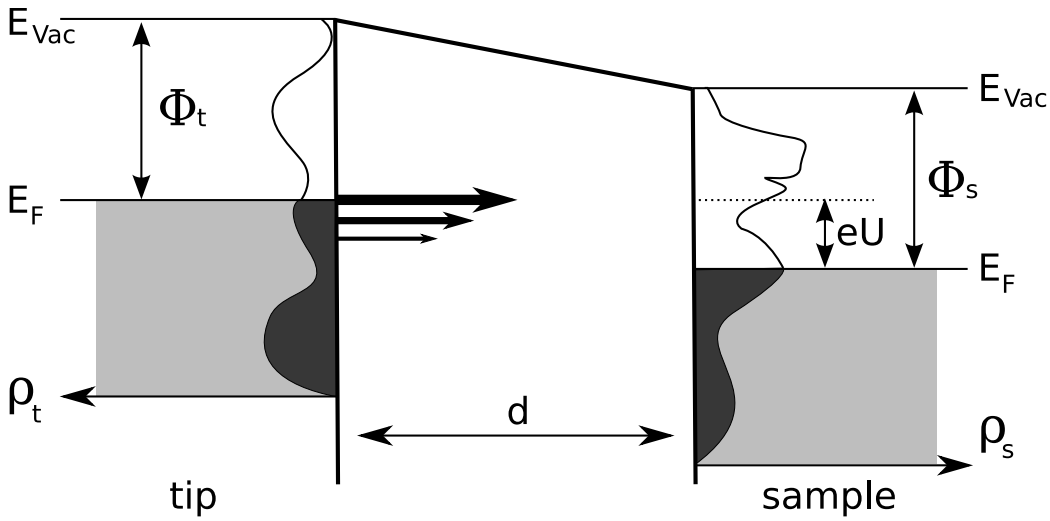

Figure 2.2: One-dimensional schematic energy diagram for tunneling from tip (grounded) to sample (positive bias voltage U applied). $\rho_{t,s}$ indicate the density of states and $\Phi_{t,s}$ the work function for the tip and the sample, respectively. The sizes of the arrows in the gap indicate that the probability for tunneling has its maximum at $E = eU$.

that in both scanning modes these maps are derived from the tunneling current and therefore resemble electronic rather than topographical features (see next section).

Mathematical Description of the Tunneling Process

Developing a precise mathematical description of the tunneling process in STM is tempting. The main problems are the unknown geometry of the tip (which may even change during one experiment) and its chemical composition. Nevertheless, applying some simplifiations and assumptions, the basic aspects of the process can be explained.

When a macroscopic partical of mass m faces a potential V_0 that is greater than its energy E, the partical is reflected. But when the partical decreases to a size, where its wave character becomes recognizable, this classical description fails. In this region, the particle can, if the barrier width d is small enough, with a small propability Q tunnel through the energetically

forbidden region and be detected on the other side (Figure 2.1).[4]

$$Q = exp(-\frac{2d}{\hbar}\sqrt{2m(V_0 - E)}) \tag{2.1}$$

In 1961 J. Bardeen discussed the tunneling process through the vacuum between two metal plates (Figure 2.2).[5] Instead of solving the Schrödinger equation for the whole system, he devided it into two independent subsytems. In this one-dimensional theory the specific geometry of the gap is ignored. Fermi's golden rule, which describes the transition rate between two quantum states, gives the propability of an electron to elastically tunnel between a sample state at the surface and a tip state. The tunneling current I is directly proportional to the number of sample states at the surface within the energy interval eU.[6] Using Bardeen's approach, it can be aproximated as[7, 8] (with the Fermi energy $E_\mathrm{F} = 0$)

$$I \propto \int_0^{eU} dE\rho_\mathrm{t}(E - eU)\rho_\mathrm{s}(E)T(E, eU, d), \tag{2.2}$$

where U is the applied small bias voltage (with respect to the tip), and $\rho_{\mathrm{t,s}}$ are the densities of states for the tip and the sample, respectively. *T(E, eU, d)* is the transmission coefficient,

$$T(E, eU, d) = exp(-\frac{2d}{\hbar}\sqrt{2m(\frac{\phi_\mathrm{t} + \phi_\mathrm{s}}{2} - \frac{eU}{2} - E)}, \tag{2.3}$$

where $\phi_{\mathrm{t,s}}$ are the work functions for the tip and the sample, respectively.

According to equation 2.2, the tunneling current is simply an integral of the transmission coefficient multiplied with the densities of states $\rho_{\mathrm{t,s}}$ (DOS) of the tip and the sample. However, this equation does not include the tip geometry. Therefore, the DOS of tip and sample are exchangable. To apply Bardeen's theory to the STM, in 1983 J. Tersoff and N. D. Hamann approximated the tip apex as a metal sphere with only the s-states of the tip applying to the tunneling process.[9, 10] According to their formula, the contribution of the tip to the tunneling current is only a constant value. Therefore, by detecting the tunneling current (equation 2.2), basically the local density of states (LDOS) of the sample is recorded. For metal surfaces, the LDOS reflects the surface topography in good agreement[5], but for adorbates there may be vast differences (see section 2.1.2).

[4] A description of the tunneling effect can be found in many textbooks, for example in Ref.[4]

[5] Although even for clean metal surfaces features like surface states lead to a difference between the topography and the LDOS.

The simple model of the Tersoff-Hamann theory failed in explaining the observed atomic resolution on close-packed metal surfaces.[11] This was achieved in 1990 by C. J. Chen, who assumed a d_{z^2}-tip state.[12, 13] A more detailed description of the tunneling process can be found in many books[6, 11] and in a review by D. Drakova.[14]

2.1.2 Imaging Molecules

The question whether it is possible to image organic adsorbates and molecules with the STM was relatively easily answered by the first successfully taken STM images in the mid 1980s.[15, 16] Until then, doubts were being uttered related to the relatively large energy gap observed between the highest occupied molecular orbital (HOMO) and the lowest unoccupied molecular orbital (LUMO) compared to the low bias voltages applied in STM. This energy gap was thought to prevent the molecules from being imaged. But since the molecular orbitals (MO) interact with the metal surface's energy band, these MOs are altered[17] such that imaging becomes possible. However, it also means that the HOMOs and LUMOs of adsorbed molecules can differ from those of isolated ones.

Many effects can influence the appearence of adsorbates in STM images[6]. Depending on the applied bias voltage, different MOs can contribute to the tunneling current. For example, on a titanium film O_2 looks like a protrusion or, counterintuitively, like a depression.[19] The adsorption site of the adsorbate on the surface has an influence on the adsorption state. For example, CO on Pt(111) appears either as a "bump" on on-top sites or as a sombrero-like shape on bridge sites.[20] Also for larger adsorbates as organic molecules the appearence in STM images can depend on the applied voltage,[21] the adsorption site,[22] but also on the surface geometry.[23] Furthermore, due to intermolecular interactions, a single molecule can look different from one embedded in a network (compare figures 3.1 and 3.2 in section 3.1.1). If the molecule diffuses or rotates much faster than the characteristic scanning speed of the STM (about a millisecond per pixel, depending on the scanning mode), it might be impossible to identify the molecule or its inner structure.[24] Also, some side-groups, like alkyl-chains attached to a porphyrin ring, can continuously change their conformation while the molecular core itself is immobile on the surface. This can lead to (partly) fuzzy appearences in STM images, when the movement of such moieties is faster than the characteristic scanning speed of the STM. Furthermore, static conformational changes of the molecule's residues can lead to different appearences of

[6] A very good discussion of these effects can be found in a review by P. Sautet.[18]

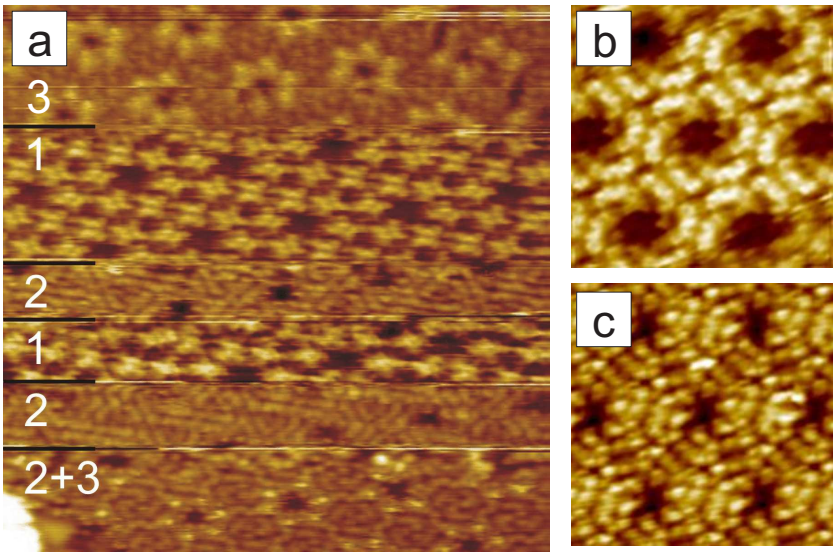

Figure 2.3: STM images of networks formed by different porphyrin derivatives showing an example for the influence of the tip on the images. a) While scanning the self-assembled network the tip was changed by applying small voltage pulses (3.5 V for 50 milliseconds). Three different imaging modes were found as labeled in the image (Image taken with $U_{\text{gap}} = -1.4$ V, $I_{\text{tunnel}} = 20$ pA, scan range: 25×25 nm^2). b) An STM image of the network formed by a different porphyrin derivative than in a) taken with mode 1 ($U_{\text{gap}} = -0.8$ V, $I_{\text{tunnel}} = 16$ pA, scan range: 7.5×7.5 nm^2). c) An STM image of the same network as in b) taken with mode 2 ($U_{\text{gap}} = -1.3$ V, $I_{\text{tunnel}} = 24$ pA, scan range: 7.5×7.5 nm^2).

the molecules even on the same surface.[25, 26]

Despite the predictions of the Tersoff and Hamann model, the tunneling current also depends on the DOS of the tip so that the tip has a high influence on STM images. Any contamination of the tip which can spontaneously occur during an STM experiment, for example by organic materials, can affect the recorded STM image (see Figure 2.3).

2.2 Substrates

As explained in section 2.1.1, in order to image organic molecules with the STM, conductive (or semi-conductive) substrates are needed. These influence the adsorption state of adsorbates in a variety of ways, so that some aspects have to be carefully considered when choosing the substrate.

The morphology of the substrate's surface atoms as well as the size of the unit cell affect the adsorption state of adsorbates as they try to minimize their energy on the surface. The morphology is mainly defined by the geometry of the surface atoms, which can form for example a twofold (rectangular) or a threefold (hexagonal) surface. Furthermore, the atomic geometry can affect the flatness of the surface. For example, (i) the (110) surface of fcc fcc copper and silver crystals exhibits alternating atomical lines with different heights and (ii) the surfaces of gold single crystals reconstruct which leads to alternating areas with different surface geometries.[27] The unit cell also depends on the atomical species. Here, even small differences can lead to different self-assembled monolayers.[23]

Another important aspect is the reactivity of the substrate's surface which determines the mobility of the adsorbates. For strongly reactive surfaces, adsorbates tend to have no mobility at all. They stick at the place, where they impinge onto the surface.[28] As this prevents intermolecular interactions, for the purpose of self-assemblies the noble metals, which are less reactive, are the most extensively used substrates. Furthermore, fresh and clean surfaces can be easily prepared for new experiments (see section 2.3).

In this work, Cu(111) has been chosen as the supporting substrate. Copper is the most reactive of the noble metals.[29] This enhances the stability of self-assembled structures, but does not suppress their mobility. The threefold surface sructure gives rise to a variety of possible adsorption geometries. The distance between two surface atoms is 2.55 Å and the height of a monoatomic step is 2.08 Å.

2.3 Sample Preparation

All experiments were performed in a two-chamber UHV system (base pressure of 1×10^{-10} mbar). As substrate for the molecular films a (111)-oriented Cu single-crystal was used (see section 2.2), which was cleaned by cycles of sputtering with Ar^+ ions and subsequent annealing at 800 K. By this procedure, flat terraces of about 100 nm in width separated by monoatomic steps are obtained. Molecular compounds were deposited by thermal evaporation from a commercial Knudsen-cell type evaporator[7] onto the Cu substrate held at room temperature. All STM measurements were done at a sample temperature between 77 K and 200 K. Temperatures larger than 77 K are reached by counter-heating of the sample. When more than one deposition of the same compound occured, the sample was heated to room temperature

[7] www.kentax.com

for the deposition and subsequently cooled to the desired temperature for measurement.

2.4 Organic Molecules

The amount of different types of organic molecules is innumerable. However, the applicability of a certain molecular compound is determined not only by the planned experiment, but also by the experimental setup and environment. Thus, molecules must exhibit some characteristics in order to be applicable in STM experiments under UHV conditions.

For the application in the *Nanolab*, the molecules must be condensed into a powder prior to the insertion into the vacuum system. The vapor pressure of the powder must be low enough that the molecules do not evaporate spontaneously into the vacuum due to the drastically reduced environmental pressure in UHV at temperatures below approximately 120°C which are needed to clean the molecular powder from contaminations. This is often problematic for molecules with a molecular weight of less than about 200 u. In order to bring the molecules onto the substrate, they must be sublimable at temperatures above 120°C. This is done by heating the molecular powder in Knudsen cells which results in a directed flux of molecules into the vacuum. Furthermore, the molecules must be stable enough not to fragment by the heating process. This usually restricts the atomic weight to a maximum of approximately 2200 u. Furthermore, if the intermolecular interactions in the powder, which are often different from those on the surface, are too strong, it might be also impossible to sublime them. In order to use molecules which are not sublimable, different approaches as *Pulse Injection*,[30] *Spray-Jet Injection*,[31] *Electrospray Deposition*[32] and others can be utilized.

2.4.1 Porphyrin Derivatives

Porphyrin molecules are a family of (metal-)organic compounds exhibiting the same core structure, namely the porphine ring (Figure 2.4[8]). This heterocyclic macrocycle is an extended π-conjugated system which absorbs light and thus porphyrins appear deeply colored. Hence their name, which is derived from the greek word $\pi o \rho \varphi \upsilon \rho \alpha$ (porphyrá) which means purple. To the porphine ring, varying functional moieties can be attached in different positions and thus the properties of the porphyrine can be greatly altered[9].

[8] Taken from http://en.wikipedia.org/wiki/Image:Porphin.png

[9] In the special case of the tetrabenzotetraazaporphyrin, the molecule is called phthalocyanine.

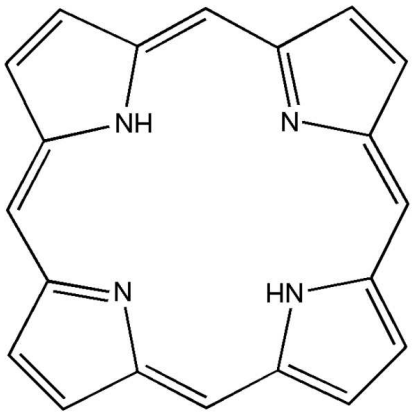

Figure 2.4: The molecular structure of the porphine ring. It consists of four pyrrole rings which are linked by methine bridges. Two of the four nitrogen atoms have a free electron. They can be either saturated by two hydrogen atoms or by a single metallic ion.

The porphine ring itself can bind different centers, like two hydrogen atoms or single metal ions with a charge of usually 2+ or 3+. In this study, the central ion is always zinc.

In nature, porphyrins are found extensively in plants, algae, cyanobacteria and in mammal blood cells. In the first, chlorophyll, a slightly changed porphine ring (chlorin) bond to a magnesium-ion, is part of the photosynthesis. Basically, the chlorophyll absorbs light and is thereby excited, which can lead to its oxidization by loosing one electron. This is one step in converting the energy supplied by light into chemical energy. In the metabolism of mammals, a protein (haemoglobin) bearing another porphyrin derivative (heme) is responsible for the oxygen transport. The central atom of the heme is an iron ion, to which the oxygen binds[10] which is then carried in the blood through the mammal's body.

In a laboratory, the first porphyrin derivatives have been synthesized in 1929[33] and in 1959 the first crystal structure of a porphyrin derivative has been reported.[34] Since then, porphyrins (and the closely related phthalocyanines) have been extensively studied and a variety of applications, as for example chemical sensors or solar cells, have been developed.[35, 36, 37] The porphyrin derivatives **P1** to **P4** which are studied in this thesis were synthesized in the group of Prof. François Diederich at the ETH Zürich. The zinc-

[10] This can be also done by myoglobin, which, however, does not specifically bind to oxygen.

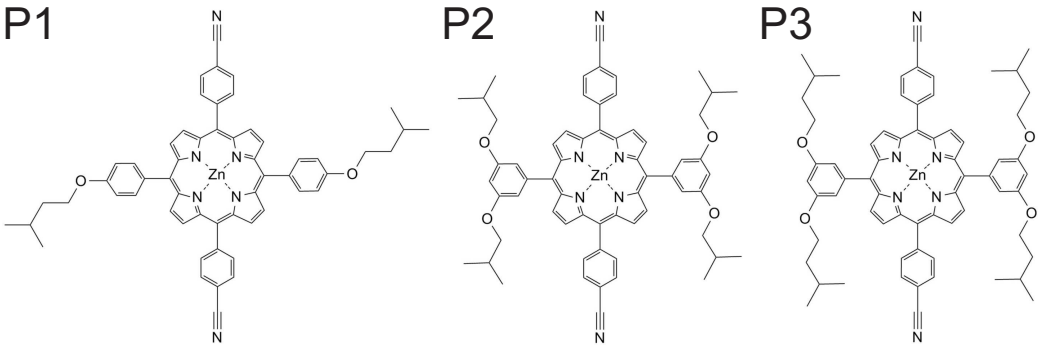

Figure 2.5: Structures of the three porphyrin derivatives **P1**, **P2** and **P3**. They were synthesized by Jens Hornung at the ETH Zürich. For a full description see section 2.4.2.

octaethyl porphyrin (**ZnOEP**) is commercially available (CAS 17632-18-7, Fluka). The structure and characteristics of these derivatives are described in the following section.

2.4.2 The Porphyrin Derivatives P1 to P4

The three derivatives **P1**, **P2**, and **P3** (Figure 2.5) were chosen for their well established linear 4-cyanophenyl group[38] which possesses a high dipole moment. This allows for strong electrostatic intermolecular coupling between adjacent molecules. The other two meso-positions of the porphyrin core are substituted with three different, flexible alkoxyphenyl substituents whose alkoxy chains differ in their length and the position in which they are attached to the phenyl ring. Specifically, these moieties are two 4-isopentoxyphenyl groups for **P1**, two 3,5-diisobutoxyphenyl groups for **P2** and two 3,5-diisopentoxyphenyl groups for **P3**. In contrast to the HOPG surface, on which alkyl chains are immobile and mainly introduced to ensure molecular self-assembly,[39] on the copper surface the alkoxy side-groups are mobile at the temperatures investigated in this study, i.e. above 77 K. They have different conformational flexibilities, and an increasing steric demand from **P1** to **P3**. Since the alkoxy-chains of **P2** and **P3** are attached in the meta-position, they can be in closer proximity to both the porphyrin core and the 4-cyanophenyl substituents compared to **P1**. Due to a steric hindrance between the hydrogens of the four phenyl rings and those of the porphyrin ring, the four moieties cannot be parallel to the porphyrin center. In fact, in the gas phase, they are rotated by an angle of 60 to 90 degrees against the porphyrin core.[23] On the metal surface, however, when the molecule is

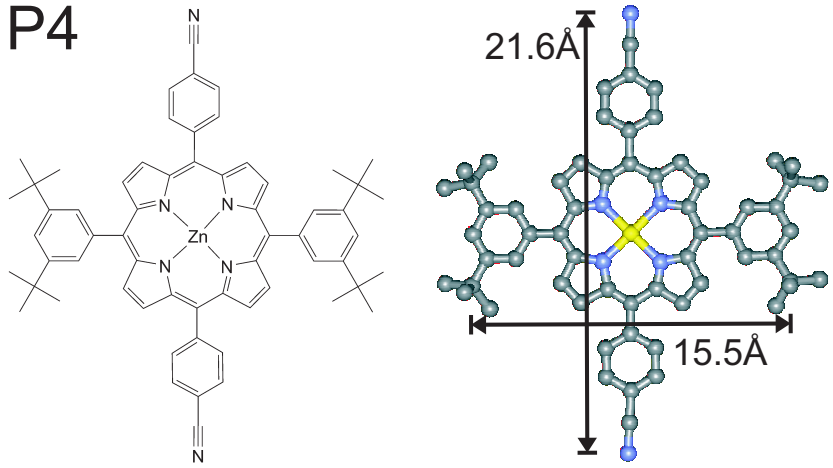

Figure 2.6: (left:) Structure of the porphyrin derivative **P4**. It was synthesized by Fuyong Cheng at the ETH Zürich. For a full description see section 2.4.2. (right:) A PM3-optimized ball-and-stick model of **P4** including some important intermolecular distances.

adsorbed in a flat lying geometry, this angle can be as small as 20 degrees due to interactions with the substrate.

The porphyrin derivative **P4** (Figure 2.6) is closely related to **P2** and **P3**. It exhibits the same 4-cyanophenyl group. However, the flexible alkoxyphenyl substituents have been exchanged by bulky di(*tert*-butyl)phenyl groups. The mobility of the *tert*-butyl groups is primarily restricted to a rotation around the bond between the phenyl ring and the center carbon atom. The intramolecular distances of **P4** have been calculated by a PM3 optimized geometry. The most important ones are shown on the right side of Figure 2.6.

2.4.3 ZnOEP

The zinc-octaethyl porphyrin (Figure 2.7) has, in contrast to the other derivatives used in this study, only one kind of moiety, namely a short ethyl chain. It is attached to the eight β-positions of the porphyrin core. Compared to the alkoxy chains described in section 2.4.2, these alkyl chains are less mobile and have less degrees of freedom.

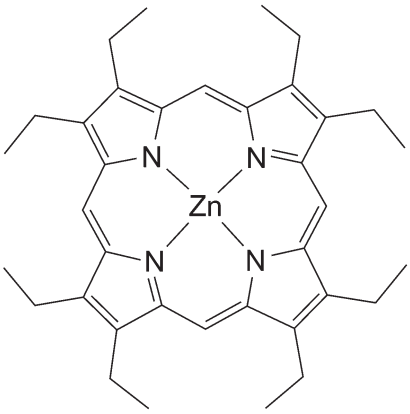

Figure 2.7: Molecular structure of the porphyrin derivative zinc-octaethyl porphyrin (**ZnOEP**).

2.5 Self-Assembly

In 1991, G. M. Whitesides described the process of molecular self-assembly as "the spontaneous association of molecules under equilibrium conditions into stable, structurally well-defined aggregates joined by noncovalent bonds."[40] Although this is not the only definition of self-assembly, it is the one that describes the effects presented in this thesis best.

Self-assembly is a widely spread phenomenon in nature. In solution, lipids self-assemble into micells or biomolecular doublelayers, which are used by nature as a protective layer that confines the inner parts of cells against the surrounding environment. Self-assembly in three dimensions is utilized to grow crystals consisting of organic materials. Organic molecules on metalic surfaces can self-assemble spontaneously into ordered structures. Because of this diversity, self-assembly is studied by Biologists, Chemists, and Physicists alike.

Thermodynamics predicts that the change of entropy[11] dS in a system can only be greater or equal to zero. However, to fully understand complex biological systems it is useful to devide dS into two parts:[41]

$$dS = dS_i + dS_e, \tag{2.4}$$

where dS_i is the inner change of entropy and dS_e is the change of entropy occuring by an exchange of heat or material with the environment. By this,

[11] Entropy is often discribed as a measure for disorder. However, for more complicated systems this description leads to the imagination that ordering cannot occur. This is obviously wrong, as innumerous examples show.

it becomes clear that a decrease of entropy inside one part of a system can be compensated by an equal or greater increase of entropy in another part of the system, for example by a rearrangement of the molecules of a solvent. However, as in UHV no solvent is present, which could balance the loss of entropy occuring in an ordering process as self-assembly, the compensation must be done otherwise, namely by a decrease of enthalpy which is done by interactions between the molecular compounds. To take account of this fact the change in *free standard enthalpy* ΔG must be considered:

$$\Delta G = \Delta H - T\Delta S, \tag{2.5}$$

where H is the *standard enthalpie*. If $\Delta G < 0$, a chemical reaction occurs spontaneously. This is obviously the case if the change of entropy $\Delta S > 0$ and $T\Delta S > \Delta H$. However, also a negative change in entropy ($\Delta S < 0$), caused by an increased ordering of the system, can lead to a spontaneous reaction if the change in H compensates for the occuring loss of entropy, so that ΔG becomes negativ. In the case of self-assembly this means that the decrease of enthalpy required to balance the losses of entropy which occurs when the molecules are immobilized, can be achieved by increased intermolecular interactions. As noncovalent interactions, like van-der-Waals interactions or hydrogen bonds, are relatively weak compared to covalent bonds, the amount of these interactions must be maximized in order to compensate for the loss of entropy. Furthermore, very flexible moieties, as the alkyl chains used in this study, exhibit a higher entropy than rigid parts, which results in an additional need for compensation of the loss of entropy.

2.6 Manipulation of Single Molecules with the STM

Soon after the first images had been taken with the STM, it turned out that interactions with the scanning tip often lead to modifications of the adsorbed species. However, this disadvantage was turned into an advantage when scientists learned how to utilize these manipulations in a controlled way.

Mainly, five different methods exist to manipulate the state of an adsorbed species.[42, 43] For the first two methods, the interactions between the tip and the adsorbate are used to laterally displace the adsorbed species. These interactions, which can be described by the well-known Lennard-Jones potential, can be either attractive or repulsive. Accordingly, when the tip is placed next to the adsorbate, it can be either pulled or pushed along the

surface. Third, in the so called *sliding mode*, the tip is placed above the adsorbate, which is "squeezed" between the tip and the surface. Thereby, a van-der-Waals trap can be created under the tip which forces the adsorbate to follow the tip's movement. Forth, the electric field between the tip and the substrate can be utilized to perform a vertical manipulation.[44] Here, the tip is placed over the adsorbate, the feedback loop is opened, and a voltage pulse is applied. Thereby, the adsorbate can be transfered to the tip. The same procedure, but with opposite voltage, can be used to place the adsorbate on the surface. Finally, the same process can be used to locally induce heat into the adsorbate. This can lead to an excitation of the adsorbate which thereby, depending on the kind of excitation, can change its state. However, not all adsorbates can be manipulated by all methods.

While there are some reports on successful manipulations on metallic surfaces, there are only a few examples of manipulations of molecules which are located inside a molecular network or in/on a second layer of molecules.[45, 46] This might be due to an increased diffusion barrier compared to the substrate, which hinders the manipulation or disrupts the underlying molecular layer, when the parameters used for the manipulation are too severe.

Chapter 3

Results

In this chapter, the results for the adsorption and co-adsorption of the different porphyrin derivatives described in section 2.4 on the threefold Cu(111) surface are presented and discussed. It is divided into three sections.

In the first part, a comparative study is presented, in which the self-assembly behavior of the three porphyrin derivatives **P1**, **P2** and **P3** is studied in detail. At low sub-monolayer coverages, the three compounds show different behaviors: **P1** self-assembles into a two-dimensional nanoporous network, while **P2** and **P3** form a one-dimensional phase consisting of molecular chains. At coverages close to a full monolayer all derivatives assemble into nanoporous networks which differ in their pore-to-pore distance and internal structure. All observed effects are explained by (i) the different steric demands of the alkoxyphenyl moieties of the three compounds and (ii) the balancing of the entropic losses of the different alkoxy chains by van-der-Waals interactions.

In the second part, a device is presented which makes use of a nanoporous network as described in the first part. A small change in the molecular structure allows the molecules to form a supramolecular multi-position device in a one-step self-assembly process. The device consists of the supporting nanoporous porphyrin network as a host for single porphyrin guests nested on top of the pores. This unprecedented structural arrangement allows the guests to rotate and snap into six different positions, of which three are distinguishable by the STM technique. By thermal activation, or by an interaction with the STM tip, the guest molecules can hop from one position into another one without leaving the hosting pore. The regular arrangement leads to the possibility of independently addressing and operating each device by labeling its position within the network as well as determining its state by detecting the alignment of the guest relative to the hosting network and the STM scanning direction.

In the third part we will investigate bimolecular systems. Two systems are presented in which two different molecular species are susequently sublimed on the same surface, respectively. Depending on their ability to mutually compensate for the occurring loss of entropy, a process which has been studied in the first part, the two systems show different bevaviors: The first system exhibits separated phases while the second system self-assembles into a mixed network consisting of both molecular derivatives. Intermixed networks have been only rarely observed so far[47, 48, 49, 50, 51, 52] and understanding their formation is another important step in gaining control over the self-assembly behavior.

3.1 Comparative Study of P1, P2 and P3

The following is a copy of the manuscript as submitted to *Small*. Please note that the derivatives **P1**, **P2** and **P3** are called molecules **1**, **2** and **3** in this manuscript.

3.1.1 Publication A

Controlling Dimensionality and Periodicity of Supramolecular Assemblies on Surfaces by Rational Modifications of Alkoxy Substituents**

N. Wintjes, J. Hornung, J. Lobo-Checa, T. Voigt, T. Samuely, C. Thilgen, M. Stöhr, F. Diederich, T. A. Jung

[*] Nikolai Wintjes, Dr. Jorge Lobo-Checa, Tomáš Samuely, Dr. Meike Stöhr
Department of Physics
University of Basel
CH-4056 Basel (Switzerland)
Fax.: +41 61 2673773
E-Mail: n.wintjes@unibas.ch

Jens Hornung, Dr. Tobias Voigt, Dr. Carlo Thilgen, Prof. Dr. François Diederich
Laboratorium für Organische Chemie
ETH-Zürich, Hönggerberg, HCI
CH-8093 Zürich (Switzerland)
Fax: (+41) 044-632-1109
E-mail: diederich@org.chem.ethz.ch

Dr. T. A. Jung
Laboratory for Micro- and Nanotechnology
Paul Scherrer Institute
CH-5232 Villigen PSI (Switzerland)
Fax: +41 56 3102646
E-Mail: thomas.jung@psi.ch

[**] This work was supported by the European Union through the Marie-Curie Research Training Network PRAIRIES, contract MRTN - CT - 2006 - 035810, the Swiss National Science Foundation and the NCCR "Nanoscale Science". We also thank the Swiss Federal Commission for Technology and Innovation, KTI, and Nanonis Inc. for the fruitful collaboration on the data acquisition system.

Supporting information for this article is available on the WWW under http://www.small-journal.org.

Keywords

entropy/enthalpy compensation - porphyrinoids - scanning probe microscopy - self-assembly - supramolecular chemistry

Abstract

The self-assembly of three porphyrin derivatives was studied in detail on a Cu(111) substrate by means of Scanning Tunneling Microscopy. All derivatives bear two 4-cyanophenyl sustituents in diagonally opposed meso-positions of the porphyrin core but differ in the other two alkoxyphenyl type substituents. At coverages below 0.8 monolayers, two derivatives form molecular chains, which evolve into nanoporous networks at higher coverages. The third derivative self-assembles directly into a nanoporous network without showing a one-dimensional phase. The pore-to-pore distances for the three networks depend on the size and shape of the alkoxyphenyl substituents. All observed effects are explained by an interplay between the steric demand of the alkoxyphenyl residues and the entropy/enthalpy balance of the network formation.

1. Introduction

Complex molecular layers on surfaces with engineered architectures and properties[1] are expected to play an important role in the development of future devices at the nanoscale.[2] In contrast to 3D crystal packing of molecules or tectons, which has been a focus of research for a long time,[3] surface and interface self-assembly allows for the addressing of individual units.[4,5] To control the self-assembly process[6] at the surface, a detailed understanding of the involved molecule-surface and intermolecular interactions is crucial. Their interplay can lead to a variety of phases for the same coverage[7,8] but the observed phases can also depend on the surface coverage.[9] In the latter case, several phases might co-exist for a small coverage region,[10] or a transition from one phase to the other occurs.[11]

Since the invention of STM in 1981, a significant number of two-dimensional patterns at the solid - liquid and the solid - vacuum interface have been reported.[12] Among them, there are some striking examples of self-assembly which are guided, for example, by solvent interactions,[13] surface pre-patterning,[14] molecular symmetry,[15] the use of elaborated binding motifs as they are found in hydrogen bonding,[16] interactions among polar groups,[17]

metal complexation,[18] or by exploiting the interactions of long alkyl chains with the underlying substrate.[19]

In view of future applications, an especially interesting field of self-assemblies are (i) molecular chains because of their potential as organic wires as well as (ii) porous networks due to their capability to recognise[20,21] and host molecular guests.[5,22] Previous work has shown that it is possible to modify the pore dimensions of such networks by completely changing the molecular building block.[8,23] So far, however, no systematic study has focused on how the variation of functional subunits ("synthons") attached to the same molecular core influences the structures of self-assembled porous layers.

The concept of synthons as formal molecular fragments with a specific reactivity was introduced by Corey[24] for the planning of covalent syntheses and has later been extended to molecular crystals and non-covalent supramolecular assemblies by Desiraju.[25] The cyanophenyl fragment[26] used in this work was initially investigated in 3D crystals[27] where it forms linear dimers and cyclic trimers[25] as distinct assemblies. In recent work, cyanophenyl derivatives have been used for the assembly of addressable supramolecular structures at surfaces where they arrange with a similar geometry in one- and two-dimensional assemblies.[4,17,20,22,28] The molecules used in the present study are derived from the well-known tetraphenyl porphyrin core[29,30] and combine the cyanophenyl synthon with alkoxy groups for additional direction in the supramolecular self-assembly process at the surface. The latter, rather apolar synthon allows to make use of hydrophobic effects that have already been discussed by Desiraju.[25] Another important feature of alkoxy residues is their tendency to condense or exhibit fluid-like dynamic behavior depending on the conditions,[31] as it is well known from liquid crystals.[32]

Here we present a systematic study on the influence of different alkoxyphenyl substituents on the resulting 2D porphyrin arrangements at solid vacuum interfaces, indicating that the concept of synthons can be transferred to the field of supramolecular surface assemblies. The architecture as well as the temperature activated mobility and corresponding steric requirement of the alkoxyphenyl residues are identified as the key parameters governing the resulting structures, i.e. one-dimensional molecular chains or two-dimensional porous layers.

2. Results and Discussion

2.1 Appearance of the Molecular Compounds in STM Images

The selected molecular compounds (**1-3**) were sublimed onto a Cu(111) substrate at sub-monolayer coverages. Consistent with earlier observations,[33] the influence of the STM tip leads mainly to two different imaging modes,

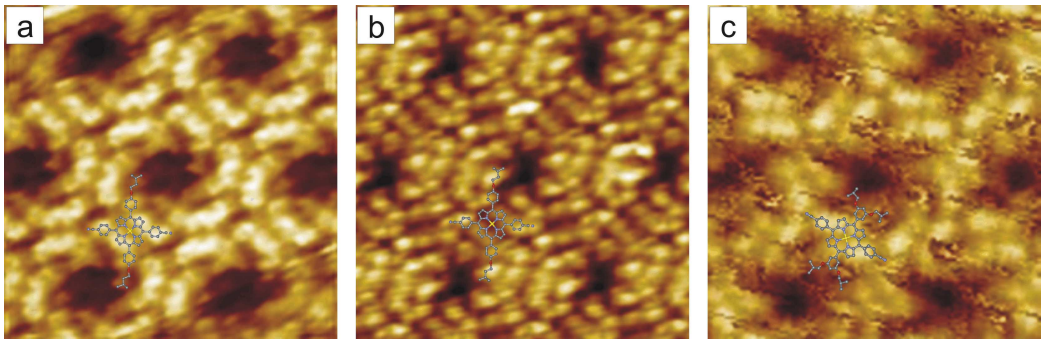

Figure 3.1: STM images (all 7.5 × 7.5 nm^2) showing the arrangement of molecules **1** (a and b) and **2** (c) on Cu(111) at coverages > 0.8 ML. Two different imaging modes could be observed depending on the tip conditions: a) The π-system of the molecules is pronounced ($U_{\text{gap}} = -0.8$ V, $I_{\text{tunnel}} = 16$ pA). b) All parts of the molecules provide equal contrast ($U_{\text{gap}} = -1.3$ V, $I_{\text{tunnel}} = 24$ pA). c) Mobile parts of the molecules can lead to characteristic streaks in STM images ($U_{\text{gap}} = -2.5$ V, $I_{\text{tunnel}} = 20$ pA).

in which either the π-system provides the dominant contrast ("π-imaging mode", Figure 3.1a), or all parts of the molecule are equally visible ("full imaging mode", Figure 3.1b). In the π-imaging mode, the porphyrin ring is imaged as two opposing lobes separated by a dark line. This appearance is caused by a saddle-shaped deformation of the porphyrin ring induced by a steric hindrance between the β-hydrogen atoms of the core and hydrogens of the phenyl rings.[34] Consequently, two pyrrole rings are tilted upwards and provide strong contrast in the STM images while the other two rings are tilted downwards and appear as a dark line. The four phenyl rings can be recognized as four lobes in close vicinity to the porphyrin ring, each providing the same contrast as the pyrrole rings that are tilted upwards. These features allow for a precise identification of an individual molecule even inside a network (see the superimposed molecular structure in Figure 3.1a). The mode of imaging is not influenced by the applied voltage. However, by using voltage pulses of around 3.5 V and 50 ms, one can sometimes switch between imaging modes (see supporting information). Hence, it is plausible that the different modes are caused by subtle changes of the tip, for example caused by an adsorbate on the tip, as likewise observed in other STM studies.[35]

Depending on the scanning conditions, sections of the STM images may show a characteristic fuzzy signal regardless of the imaging mode (Figure 3.1c[36]). These streaks can be related to parts of the molecules that move

while being passed by the scanning tip.[37] For the present systems, we attribute this effect to the mobility of the alkoxy chains. The streaks diminish with increasing proximity of tip and sample. This can be associated with an increasing interaction between the scanning tip and the molecular chains which are thereby pushed aside.[38]

2.2 Self-assembly Behavior at low Sub-Monolayer Coverage

For molecule **1** we observed self-assemby to a nanoporous, hexagonal network with P3 symmetry at coverages < 0.05 ML (Figures 3.1a and 3.1b), after the well-known initial decoration of the step edges.[39] This network exhibits the same internal geometry as previously published porphyrin assemblies[22] and will be described in detail in section 2.5. In contrast, molecules **2** and **3** form long chains with the same characteristics after decorating the step edges and for molecular coverages up to approximately 0.8 ML, (Figure 3.2a). The chains nucleate either at one of the molecules decorating the step edges or at a defect on a terrace and are stable up to at least 200 K. At room temperature molecules are observed in a 2D mobile phase.[40]

Within the chains, a single molecule can be clearly identified (Figure 3.2b, top). The porphyrin core and the phenyl rings appear as described above for the π-imaging mode. The cyano group is not resolved. The alkoxy chains appear as one lobe each, situated above and below the porphyrin ring and the 4-cyanophenyl substituents. No significant difference in the appearance of molecules **2** and **3** was found in the STM images.

A closer analysis reveals that the chains exhibit mainly two interconnecting modes for adjacent molecules. The first one is a straight connection which simply prolongates the chain (circle a in Figure 3.2a). The second one leads to a kink (circle b), which changes the direction of the chain, mostly by ca. 30 degrees. Often, sections are found in which a kink towards one side is immediately followed by a kink towards the other side, leading to a zig-zag type, overall straight section (circle c).

Most probably, in a straight connection, the cyano groups, which are not visible in the STM image, are lying anti-parallel and interact via dipole-dipole interactions (as shown for molecules no. 3 and 4 in Figure 3.2b[41]). This type of interaction was theoretically described by Y. Okuno et al. for a benzonitrile dimer[42] and is also known in the gas phase[43] as well as in organic crystals.[44] Sometimes, a small variation of this bonding motif can be found, as seen for molecules no. 1 and 2 in Figure 3.2b. Here, the molecules in a straight section are lying closer together and show a small vertical and lateral displacement. Our calculations[41] indicate that this is due to a weak hydrogen bond between the cyano group and the β-hydrogens of the porphyrin ring, as indicated by the molecular model in the lower part of Figure 3.2b.

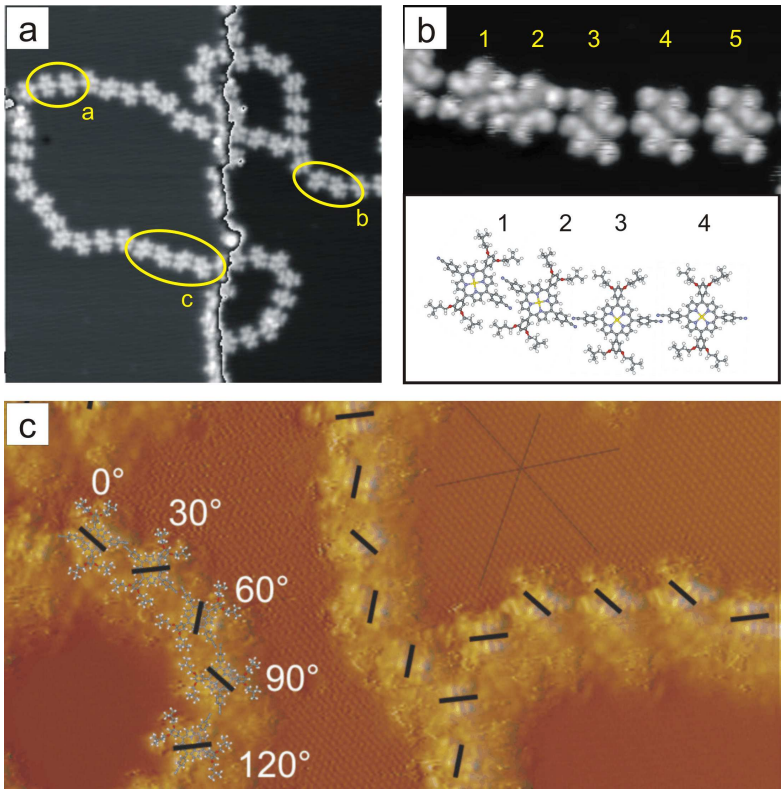

Figure 3.2: STM images showing the arrangement of molecules **2** (a and b) and **3** (c) on Cu(111) at coverages < 0.8 ML (see also supporting information). Both molecules arrange in chainlike structures. Individual molecules can be clearly identified. a) STM image showing a typical chain formed by molecule **2** (41×41 nm^2; $U_{\mathrm{gap}} = -1.5$ V, $I_{\mathrm{tunnel}} = 20$ pA; The color-scale of the image was adjusted to provide good contrast on the terraces for highlighting the molecular features. A step edge, seen in the image as a black line, runs vertically from top to bottom). b) Top: A detailed STM image showing the main types of connections between adjacent molecules in the molecular chains (12×6 nm^2; $U_{\mathrm{gap}} = -1.6$ V, $I_{\mathrm{tunnel}} = 11$ pA). Bottom: A tentative model, generated with Spartan[41] for the intermolecular interactions within the chains. c) Simultaneous imaging of molecular chains of **3** and substrate atoms of Cu(111). The orientation of the characteristic dark lines (see description in the main text) is marked by black lines which allow for an easy correlation with the principal directions of the substrate.

Within the kinks the dipole-dipole interaction is weakened, as the dipoles are not perfectly anti-parallel in such an arrangement (molecules no. 2 and 3 in

Figure 3.2b). Nevertheless, this loss in interaction energy may be partially compensated by van der Waals interactions of the alkoxy chains[45] which are closer together than in the straight sections.

2.3 Influence of the Underlying Cu(111) Surface on the Porphyrin Chain Formation

In vacuum the substituents of tetra-aryl porphyrins can perform a hindered rotation depending on the temperature.[46] After adsorption on the metal surface, however, the rotational angle of such moieties is typically fixed in a position which depends on the interaction with the substrate.[30] Consequently, two conformational enantiomers, corresponding to a positive or negative tilt angle of the alkoxyphenyl substituents are observed upon adsorption. In STM images, these can be distinguished by the relative orientation (+45 degrees or -45 degrees) of the characteristic diagonal dark line with regard to the cyanophenyl substituents. The two conformational enantiomers are found with equal probabilities for all three porphyrins studied here, which is in agreement with earlier observations.[47] Achiral conformers exhibiting parallel rotation of the opposite aryl-porphyrin bond which are also possible for symmetry reasons, have not been identified in our study. By analyzing STM images that exhibit both good resolution of the adsorbed molecules and atomic resolution of the substrate (Figure 3.2c), it can be seen that the characteristic dark lines are also aligned with the main atomic directions of the supporting substrate, within an accuracy of ± 7 degrees. This observation, in combination with the two possible orientations of the dark line with respect to the cyanophenyl-cyanophenyl axis, can explain the changes in direction of 30 degrees within a kink: Two different enantiomers, which are adjacent within a chain and are aligned along different principal directions of the threefold symmetric (111) substrate, exhibit a relative orientation of $120 - (45 + 45) = 30$ degrees. In contrast, adjacent but identical enatiomers which are aligned along the same principal directions form a straight connection. In the STM images, this is revealed by the observation that in a straight connection, two adjacent molecules look like perfect copies of each other (with the same orientation of the dark lines) while in a kink, they appear as mirror images. For two-dimensional assemblies of similar porphyrin derivatives, long-range interactions that extend beyond nearest neighbors have also been reported.[20] However, no clear evidence for such interactions was found here, since they should lead to a preferred arrangement with either straight, curved, or zig-zagged chain sections.

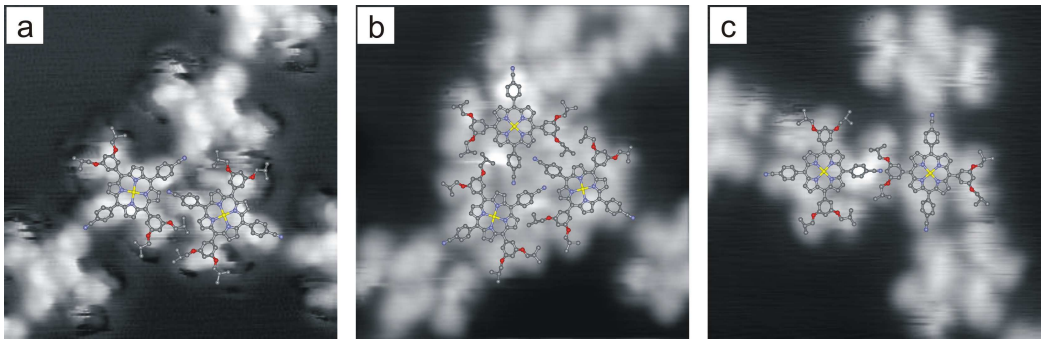

Figure 3.3: High-resolution STM images (all 6.4 × 6.4 nm^2; U_{gap} = −1.5 V, I_{tunnel} = 20 pA) of molecule **2** on Cu(111) showing different types of branching points for the molecular chains. Types a) and c) can be also found for molecule **3**. a) Branching by hydrogen bond formation between the cyano group of one molecule and either the porphyrin core or the 4-cyanophenyl substituent of another molecule. b) Similar interactions as in a) but in a trimeric arrangement. c) Branching by a hydrogen bond formation between the cyano group of one molecule and the phenylene ring of the alkoxyphenyl substituent of another molecule.

2.4 Branching of the Porphyrin Chains

Next to the two types of intermolecular connections observed in linear chain sections, two distinctly different types of branching arrangements were found (Figure 3.3). As to the first, a cyano group of one molecule forms a hydrogen bond either with a β-hydrogen of the porphyrin core or with a hydrogen atom of a 4-cyanophenyl ring of another molecule (Figure 3.3a). This motif has been found for both molecules **2** and **3**. In addition, the formation of a symmetric cyclic trimer was observed exclusively for molecule **2**. Within the trimeric structure, a cyanophenyl group of each molecule acts as hydrogen bond acceptor towards one and as a donor towards the other partner, thereby interconnecting three molecules by three hydrogen bonds (Figure 3.3b). Similar trimeric arrangements have been reported in literature for cyanophenyl derivatives in the gas phase,[43] in two-dimensional assemblies,[22,28,42] and also in 3D crystal structures.[48] In the second branching arrangement, the 4-cyanophenyl group of one molecule forms a hydrogen bond with the phenylene ring of the bis(alkoxy)phenyl substituent of a second molecule (Figure 3.3c). This type is again observed for both molecules **2** and **3**.

2.5 Self-assembly Behavior at High Sub-Monolayer Coverages: Tailored Nanoporous Networks

Above a coverage of approximately 0.8 ML all studied molecules (**1**-**3**) self-assemble into nanoporous, hexagonal networks with P3 symmetry. We were able to develop a tentative model for each of the three networks, guided by the following aspects: First, we compared the networks observed in the present study to a network previously reported by our group, which is formed by a similar porphyrin derivative.[22] Second, we took advantage of the π-imaging mode which allowed for a reliable identification of single molecules inside the network. Finally, we related the fuzzy parts observed in some STM images (see above) with the alkoxy chains.

The nanoporous network formed by molecule **1** (we will refer to it as network **1**; Figure 3.4a, left) exhibits a pore-to-pore distance of (30.9 ± 2.0) Å. The unit cell contains one pore and three molecules. The model (Figure 3.4a, right) reveals that the pores are chiral. Thus, two types of homochiral domains can be found on the copper surface[49] due to a separation of the two different conformational enantiomeres. Each pore is formed by the alkoxy chains of six different molecules, each of which is part of two neighboring pores. The network is stabilized by two features. First, the apolar alkoxy chains are found inside the pores and are thereby separated from the polar 4-cyanophenyl groups. Second, the 4-cyanophenyl group of one molecule points towards the porphyrin core of an adjacent molecule, forming a hydrogen bond. This bonding type is exploited by three molecules to form a trimer (blue solid circle in Figure 3.4a).

Molecule **2** forms a network (we will refer to it as network **2**; Figure 3.4b, left) with a pore-to-pore distance of (33.5 ± 1.2) Å which is slightly larger (about 8%) than that of network **1**. Again, the unit cell contains one pore and three molecules per unit cell. According to the model (Figure 3.4b, right), the structures of network **2** and network **1** are similar: Each pore is surrounded by six molecules, with each molecule being shared by two pores. Polar and apolar groups are separated. The main difference between networks **1** and **2** is that in the latter case, cyano groups point towards the hydrogen atoms of the 4-cyanophenyl ring of an adjacent molecule instead of to the hydrogen atoms of its porphyrin core. This interaction type is the same as that found for the branching mechanism shown in Figure 3.3a. The space required for this motif is slightly higher than for the similar arrangement in network **1** (cf. the blue circles in Figure 3.4a and b), which explains why the pore-to-pore distance in network **2** is slightly larger than in network **1**. The formed trimers (blue solid circle in Figure 3.4b) are identical to those observed in the chains (Figure 3.3b).

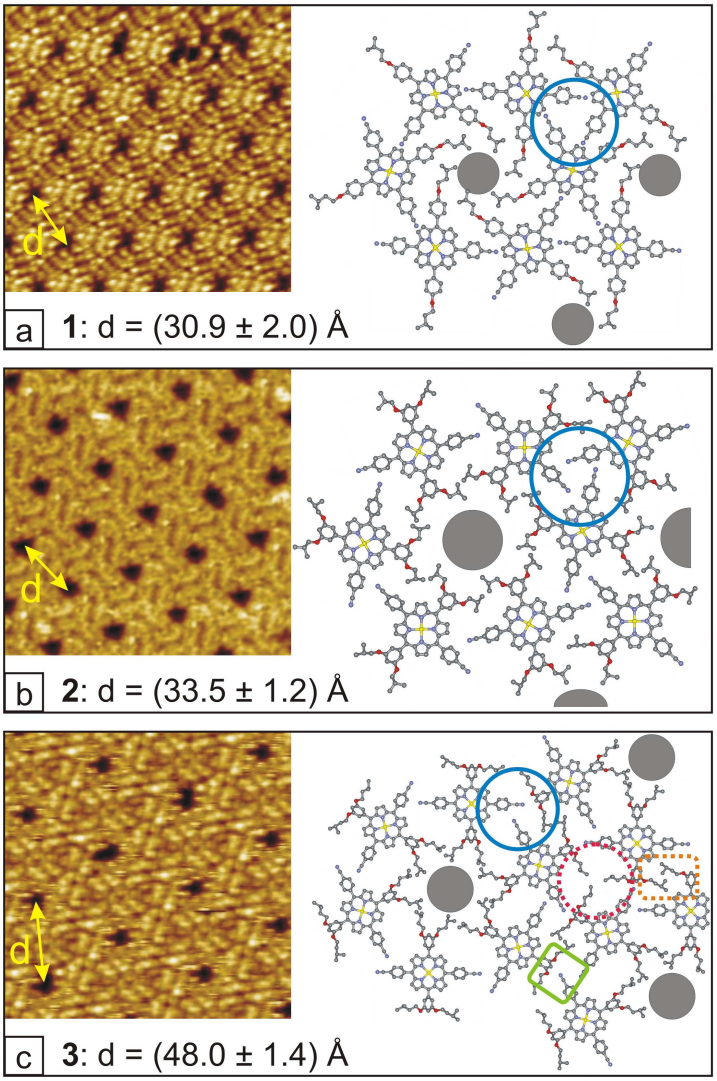

Figure 3.4: left: STM images (all 15×15 nm^2); a) $U_{\text{gap}} = -1.3$ V, $I_{\text{tunnel}} = 24$ pA; b) $U_{\text{gap}} = -1.5$ V, $I_{\text{tunnel}} = 20$ pA; c) $U_{\text{gap}} = -0.4$ V, $I_{\text{tunnel}} = 17$ pA) of the nanoporous networks formed by the three different porphyrin derivatives at coverages close to one monolayer. The networks exhibit different pore-to-pore distances d. right: Tentative models of the three networks. The filled gray circles indicate the positions of the pores. The colored circles and rectangles indicate different bonding arrangements stabilizing the network (see text for details). The pores in c) exhibit characteristic streaks, indicating mobility of the alkoxy chains.

Molecule **3**, which differs from molecule **2** only by the increased length of the alkoxy chains, forms a network (referred to as network **3**; Figure 3.4c, left) with a pore-to-pore distance of (48.0 ± 1.4) Å which is significantly larger than the distances in networks **1** and **2** (by about 43% and 55%, respectively). Remarkably, in this network the unit cell still contains one pore, whereas the number of molecules enclosed is doubled to six molecules. As a common characteristic, a single pore is formed by six molecules (Figure 3.4c, right). The cyano groups point towards the phenylene ring of an adjacent molecule, similar to network **2**. But unlike in the other two networks, each molecule belongs distinctly to one pore which leads to the significantly larger pore-to-pore distance. The molecules of neighboring pores interact with each other in a similar way as in the branching mechanism shown in Figure 3.3c (green solid rectangle in Figure 3.4c). Thus, in contrast to networks **1** and **2**, no symmetric trimer but a trimer-like motif is observed, in which one cyano group does not bind to a neighboring 4-cyanophenyl group, but forms a hydrogen bond with the phenyl ring of a bis(alkoxy)phenyl substituent (blue solid circle). Notably, polar and apolar groups are not completely separated in this network. The alkoxy chains, which are found outside the pores, interact via van-der-Waals forces and can thereby aid to stabilize the network (red dashed circle and orange dashed rectangle). They form an apolar pocket which can hardly be seen in the STM images (red dashed circle).

2.6 Thermodynamic Considerations for the Network Formations

As already pointed out by G. M. Whitesides,[50] self-assembled structures are formed by reversible association of the molecular building blocks, thereby representing thermodynamic minima. To explain the phenomena described in this manuscript, one has to take into account the different energy contributions guiding the formation of the networks and chains on the surface. First of all, depending on the strength of moleculesurface and intermolecular interactions, organic adsorbates on surfaces tend to maximize the coverage (molecules per area) and even a rearrangement into a new phase can be preferred over a second layer arrangement.[40,51] Next, due to the considerably weaker intermolecular interaction energies in the supramolecular aggregates, when compared to covalent bonding, the interplay of entropy and enthalpy is of much higher importance here.[50] Finally, on threefold symmetric surfaces, the 4-cyanophenyl group is known to favor a dimeric arrangement with anti-parallel dipoles, or a cyclic trimer.[28,42] Due to the complexity of the presented systems, accurate numerical calculations are not yet straightforward. However, the observed structures have to correspond to an energetically optimized interplay of the aforementioned contributions.

Network **1** (Figure 3.4a) features different remarkable characteristics: Although it is a porous phase, the fraction of covered surface area, as determined from STM images, is $> 90\%$. Due to the combination of a polar and a less polar synthon, a segregation occurs in analogy to the hydrophobic effect:[25] The apolar alkoxyphenyl substituents are located inside the pores and, thus, are separated from the polar cyanophenyl substituents. As a consequence, the alkoxy chains interact with each other via van-der-Waals forces while, outside the pores, the cyano groups of one molecule can form hydrogen bonds with the β-hydrogen atoms of the porphyrin core of an adjacent molecule. This results in the favored trimeric arrangement shown in Figure 3.4a (blue circle). Network **1** exhibits the densest structure ((0.36 ± 0.05) molecules per nm^2) of the three studied networks (Figure 3.4).

The formation of the network can be hindered by restricting the access of potential binding partners to the hydrogen atoms of the pyrrole units and the 4-cyanophenyl rings. This was the main idea behind the design of molecules **2** and **3**, which was implemented by attaching two alkoxy chains instead of one (cf. molecule **1**) to the phenyl substituent. In consequence, **2** and **3** do not assemble into a network at low coverage, but instead form chains via anti-parallel dipole-dipole interactions. By comparing this behavior to that of molecule **1**, which readily forms trimeric structures instead of the also possible dimers even at low coverage, we concluded the following: Without steric hindrance by an additional substituent, for the 4-cyanophenyl group the dipole-dipole interaction is energetically less favored than the formation of trimers via hydrogen bonding. This is in agreement with a calculation of Okuno et al.[42] and was also observed for a different molecular structure with similar substituents.[52]

With increasing density of the molecules on the surface, also the number of branches in the chains rises (see supporting information). Since the branching motifs of the chains can also be found in the networks, we assume that the growth of the network originates from the branching points once a critical ratio between the number of molecules and the free surface area is reached. In fact, STM images reveal that the transition from the chains to the networks starts with the formation of single pores (see supporting information).

In similarity to network **1**, the apolar alkoxy chains in network **2** (Figure 3.4b) are separated from the polar cyano groups and situated inside the pores. This arrangement is possible even though the number of alkoxy chains per molecule **2** increased by a factor of two compared to **1**. However, the correspondingly higher packing density inside the pores restricts the mobility of the alkoxy chains. To make this possible, the van-der-Waals interactions between the alkoxy chains have to compensate for the according loss of entropy.[53] The polar cyano groups again form a trimeric structure

(blue circle in Figure 3.4b). However, the β-hydrogens of the porphyrin core cannot act as hydrogen bond donors because the increased steric demand of the alkoxy chains prevents adjacent molecules to be as close as it is the case in network **1**. Therefore, the cyano group forms a hydrogen bond with the hydrogen atoms of the 4-cyanophenyl group. This results in a larger pore-to-pore distance and a decreased density of network **2** ((0.31 ± 0.02) molecules per nm^2) compared to network **1**.

As described above, we assume that the formation of network **3** nucleates from chain intersection which form a single pore. However, it appears that the even higher steric demand of the alkoxy chains of **3** as compared to **2** does not allow for the formation of a 4-cyanophenyl-based trimeric structure which is characteristic for networks 1 and **2**. In network **3** only two molecules associate via CN$\cdots$H(Ar) hydrogen bonding. Therefore we assume that there is not enough room for a third molecule to participate in a symmetric trimeric arrangement similar to the case of network **1** and **2**. Instead, a hydrogen bond is formed between the bis(alkoxy)phenyl ring of the third molecule and a cyano acceptor group of the other two, as shown in Figure 3.3c. In this new, asymmetric configuration, the alkoxy chains do not interfere with each other. The third molecule is then starting point for a second pore. Due to this uncommon asymmetric configuration, half of the alkoxy chains of each molecule are found outside the pores. This leads to an even stronger restriction of their mobility, presumably amplified by an increased interaction with the substrate, and a concomitant loss of entropy which becomes evident in the STM images by the absence of streaks (Figure 3.4c, left) for those alkoxy chains situated outside the pores (Figure 3.4c, right, dashed circle and rectangle). As in networks **1** and **2**, the model reveals a tendency for the apolar alkoxy chains to associate, either by forming pores, in which they are still mobile, or by condensation outside the pores, thereby increasing the amount of van der Waals interactions in the network. The density of network **3** is (0.30 ± 0.02) molecules per nm^2, which is comparable to that of network **2**.

3. Summary and Conclusions

By systematically varying the steric bulk of the ether substitutents of a bis(alkoxypenyl)bis(cyanophenyl)porphyrin, we showed how a gradual change in the molecular architecture influences the resulting assembly on Cu(111) at different surface coverages. In particular, a variation of the alkoxy chains in size (chain length), number and position allowed to control the dimensionality of the resulting structure, i.e. one-dimensional wires or two-dimensional porous networks, as well as the pore-to-pore distance in these networks without significantly affecting the pore diameter. We observed an increasingly

complex interplay of bonding motifs in these networks connected with the increased steric demand of the substituent. This behavior is discussed in terms of the compensation of entropic losses due to increased restriction of the flexibility of the alkoxy chains with increasing size by enthalpic interaction energies. This phenomenon is of general importance in the self assembly of thermodynamically controlled systems such as the folding of biomolecules in a cellular fluid.[54] It should be noted that for biomolecular self-assembly, solvation/hydration processes considerably affect the thermodynamics,[55] which is not the case for the dry, 'in-vacuo' assemblies studied here.

Future work will aim at the exploitation of other synthons known from supramolecular chemistry, directed towards supramolecular surface assemblies. In particular, the controlled change of the pore diameter, which might be possible by a sophisticated variation of both synthons (cyanophenyl and alkoxyphenyl) used in this study would be the next step to build more complex, addressable supramolecular structures with well-defined properties, far beyond the currently established toolbox.

4. Experimental section

4.1 Synthesis

Three different zinc porphyrin derivatives (**1-3**) were synthesized by condensation of 5-(4-cyanophenyl)dipyrromethane with the corresponding alkoxybenzaldehydes and subsequent insertion of Zn^{2+} (see supporting information).[56] Each of the resulting porphyrins was substituted with two 4-cyanophenyl groups in diagonally opposed meso-positions and two alkoxyphenyl groups in the remaining two meso-positions (Scheme 1[12]). The steric demand of the alkoxyphenyl groups (4-isopentoxyphenyl (**1**), 3,5-diisobutoxyphenyl (**2**), and 3,5-diisopentoxyphenyl (**3**)) was varied as a function of their length and branching to guide the self-assembly in a controllable way. Since the alkoxy substituents of **2** and **3** are attached to the meta-position of the connecting benzene ring, they are in closer proximity to the porphyrin core and the 4-cyanophenyl groups as compared to molecule **1**. Whereas alkyl chains adsorbed on HOPG (Highly Ordered Pyrolytic Graphite) are immobile and introduced mainly to ensure molecular self-assembly,[57] the alkoxy groups on copper are mobile at the investigated temperatures.

[12]Scheme 1 is identical to Figure 2.5 in section 2.4.2 of this thesis.

4.2 Thermal Stability of Molecules 1-3 During Sublimation

Large organic molecules often decompose under the conditions of UHV sublimation (See supporting information). To verify the thermal stability of molecules **1-3**, sublimation tests were performed prior to the STM experiments at 10^{-5} mbar in a tailor-made sublimation apparatus including a turbomolecular vacuum pump and a liquid tin heating bath. In a typical experiment, 1 mg of the molecular compound was sublimed at bath temperatures between 380 and 420°C within 10-30 min. ^{1}H NMR spectroscopic and mass spectrometric analysis of the sublimed compounds confirmed that porphyrin derivatives **1-3** sublime without fragmentation.

4.3 STM Experiments

All experiments were performed in a two-chamber UHV system (base pressure of 1×10^{-10} mbar). As substrate for the molecular films a (111)-oriented Cu single-crystal was used, which was cleaned by cycles of sputtering with Ar+ ions and subsequent annealing at 800 K. By this procedure, flat terraces of about 100 nm in width separated by monoatomic steps are obtained. The molecular compounds were deposited by thermal evaporation from a commercial Knudsen-cell type evaporator[58] onto the Cu substrate held at room temperature. In this study, the surface coverage is defined by the fraction of the surface area occupied by the deposited molecules. This can be directly determined from STM images due to the lack of a co-existing phase or a gas phase. All STM measurements were done at a sample temperature between 77 K and 200 K. Temperatures > 77 K were reached by PID-controlled counter-heating of the sample.

References

[1] J. V. Barth, *Annu. Rev. Phys. Chem.* **2007**, *58*, 375.

[2] http://www.itrs.net/reports.html

[3] a) G. Desiraju, *Crystal Engineering: The Design of Organic Solids*, Elsevier, New York, **1989**; b) M. W. Hosseini, *Accounts Chem. Res.* **2005**, *38*, 313.

[4] D. Bonifazi, H. Spillmann, A. Kiebele, M. de Wild, P. Seiler, F. Y. Cheng, H. J. Güntherodt, T. Jung, F. Diederich, *Angew. Chem.* **2004**, *116*, 4863; *Angew. Chem. Int. Ed.* **2004**, *43*, 4759.

[5] M. Wahl, M. Stöhr, H. Spillmann, T. A. Jung, L. H. Gade, *Chem. Commun.* **2007**, 1349.

[6] J.-M. Lehn, *Supramolecular Chemistry*, VCH, Weinheim, **1995**.

[7] a) K. Morgenstern, S. W. Hla, K. H. Rieder, *Surf. Sci.* **2003**, *523*, 141; b) J. Y. Grand, T. Kunstmann, D. Hoffmann, A. Haas, M. Dietsche, J. Seifritz, R. Möller, *Surf. Sci.* **1996**, *366*, 403.

[8] S. Stepanow, N. Lin, J. V. Barth, K. Kern, *J. Phys. Chem. B* **2006**, *110*, 23472.

[9] a) M. Stöhr, M. Wahl, C. H. Galka, T. Riehm, T. A. Jung, L. H. Gade, *Angew. Chem.* **2005**, *117*, 7560; *Angew. Chem. Int. Ed.* **2005**, *44*, 7394; b) G. E. Poirier, *Langmuir* **1999**, *15*, 1167; c) B. Xu, C. G. Tao, E. D. Williams, J. E. Reutt-Robey, *J. Am. Chem. Soc.* **2006**, *128*, 8493.

[10] C. B. France, P. G. Schröder, J. C. Forsythe, B. A. Parkinson, *Langmuir* **2003**, *19*, 1274.

[11] J. V. Barth, J. Weckesser, G. Trimarchi, M. Vladimirova, A. De Vita, C. Z. Cai, H. Brune, P. Günter, K. Kern, *J. Am. Chem. Soc.* **2002**, *124*, 7991.

[12] a) T. Fritz, M. Hara, W. Knoll, H. Sasabe, *Mol. Cryst. Liq. Cryst. A* **1994**, *252*, 561; b) C. Ludwig, B. Gompf, J. Petersen, R. Strohmaier, W. Eisenmenger, *Z. Phys. B Con. Mat.* **1994**, *93*, 365; c) E. I. Altman, R. J. Colton, *Phys. Rev. B* **1993**, *48*, 18244; d) M. Kunitake, N. Batina, K. Itaya, *Langmuir* **1995**, *11*, 2337.

[13] a) M. Lackinger, S. Griessl, W. A. Heckl, M. Hietschold, G. W. Flynn, *Langmuir* **2005**, *21*, 4984; b) F. Tao, S. L. Bernasek, *Langmuir* **2007**, *23*, 3513.

[14] K. Aït-Mansour, P. Ruffieux, W. Xiao, P. Gröning, R. Fasel, O. Gröning, *Phys. Rev. B* **2006**, *74*, 195418.

[15] K. Tahara, S. Furukawa, H. Uji-I, T. Uchino, T. Ichikawa, J. Zhang, W. Mamdouh, M. Sonoda, F. C. De Schryver, S. De Feyter, Y. Tobe, *J. Am. Chem. Soc.* **2006**, *128*, 16613.

[16] a) M. Ruiz-Osés, N. Gonzalez-Lakunza, I. Silanes, A. Gourdon, A. Arnau, J. E. Ortega, *J. Phys. Chem. B* **2006**, *110*, 25573; b) M. E. Cañas-Ventura, W. Xiao, D. Wasserfallen, K. Müllen, H. Brune, J. V. Barth, R. Fasel, *Angew. Chem.* **2007**, *119*, 1846; *Angew. Chem. Int. Ed.* **2007**, *46*, 1814; c) J. A. Theobald, N. S. Oxtoby, M. A. Phillips, N. R. Champness, P. H. Beton, *Nature* **2003**, *424*, 1029.

[17] H. Spillmann, A. Kiebele, M. Stöhr, T. A. Jung, D. Bonifazi, F. Y. Cheng, F. Diederich, *Adv. Mater.* **2006**, *18*, 275.

[18] a) S. Stepanow, M. Lingenfelder, A. Dmitriev, H. Spillmann, E. Delvigne, N. Lin, X. B. Deng, C. Z. Cai, J. V. Barth, K. Kern, *Nat. Mater.* **2004**, *3*, 229; b) A. Dmitriev, H. Spillmann, N. Lin, J. V. Barth, K. Kern, *Angew. Chem.* **2003**, *115*, 2774; *Angew. Chem. Int. Ed.* **2003**, *42*, 2670.

[19] S. De Feyter, F. De Schryver, in *Supramolecular Dye Chemistry* **2005**, Vol. *258*, pp. 205.

[20] A. Kiebele, D. Bonifazi, F. Y. Cheng, M. Stöhr, F. Diederich, T. Jung, H. Spillmann, *ChemPhysChem* **2006**, *7*, 1462.

[21] M. Stöhr, M. Wahl, H. Spillmann, L. H. Gade, T. A. Jung, *Small* **2007**, *3*, 1336.

[22] N. Wintjes, D. Bonifazi, F. Cheng, A. Kiebele, M. Stöhr, T. Jung, H. Spillmann, F. Diederich, *Angew. Chem.* **2007**, *119*, 4167; *Angew. Chem. Int. Ed.* **2007**, *46*, 4089.

[23] S. Stepanow, N. Lin, D. Payer, U. Schlickum, F. Klappenberger, G. Zoppellaro, M. Ruben, H. Brune, J. V. Barth, K. Kern, *Angew. Chem.* **2007**, *119*, 724; *Angew. Chem. Int. Ed.* **2007**, *46*, 710.

[24] E. J. Corey, *Pure Appl. Chem.* **1967**, *14*, 19.

[25] G. R. Desiraju, *Angew. Chem.* **1995**, *107*, 2541; *Angew. Chem. Int. Ed.* **1995**, *34*, 2311.

[26] a) S. Lee, A. B. Mallik, D. C. Fredrickson, *Crystal Growth & Design* **2004**, *4*, 279; b) R. Paulini, K. Müller, F. Diederich, Angew. Chem. 2005, 117, 1820; *Angew. Chem. Int. Ed.* **2005**, *44*, 1788.

[27] a) M. S. K. Dhurjati, J. Sarma, G. R. Desiraju, *J. Chem. Soc. Chem. Comm.* **1991**, 1702; b) P. M. Ivanov, *J. Mol. Struct.* **1998**, *440*, 121.

[28] T. Yokoyama, S. Yokoyama, T. Kamikado, Y. Okuno, S. Mashiko, *Nature* **2001**, *413*, 619.

[29] a) T. A. Jung, R. R. Schlittler, J. K. Gimzewski, H. Tang, C. Joachim, *Science* **1996**, *271*, 181; b) F. Moresco, G. Meyer, K. H. Rieder, H. Tang, A. Gourdon, C. Joachim, *Appl. Phys. Lett.* **2001**, *78*, 306; c) C. Loppacher, M. Guggisberg, O. Pfeiffer, E. Meyer, M. Bammerlin, R. Luthi, R. Schlittler, J. K. Gimzewski, H. Tang, C. Joachim, *Phys. Rev. Lett.* **2003**, *90*, 066107; d) F. Moresco, G. Meyer, K. H. Rieder, H. Ping, H. Tang, C. Joachim, *Surf. Sci.* **2002**, *499*, 94.

[30] T. A. Jung, R. R. Schlittler, J. K. Gimzewski, *Nature* **1997**, *386*, 696.

[31] a) D. Vollhardt, *J. Phys. Chem. C* **2007**, *111*, 6805; b) F. Charra, J. Cousty, *Phys. Rev. Lett.* **1998**, *80*, 1682.

[32] M. I. Boamfa, M. W. Kim, J. C. Maan, T. Rasing, *Nature* **2003**, *421*, 149.

[33] S. Weigelt, C. Busse, L. Petersen, E. Rauls, B. Hammer, K. V. Gothelf, F. Besenbacher, T. R. Linderoth, *Nat. Mater.* **2006**, *5*, 112.

[34] T. Yokoyama, S. Yokoyama, T. Kamikado, S. Mashiko, *J. Chem. Phys.* **2001**, *115*, 3814.

[35] M. Schmid, H. Stadler, P. Varga, Phys. Rev. Lett. 1993, 70, 1441; L. Bartels, G. Meyer, K. H. Rieder, *Surf. Sci.* **1999**, *432*, L621.

[36] We show an image of the network formed by molecule 2 here, because we feel it demonstrates the described fuzziness best. Nevertheless, the effect can be observed for all shown molecules.

[37] M. Wahl, M. von Arx, T. A. Jung, A. Baiker, *J. Phys. Chem. B* **2006**, *110*, 21777.

[38] T. Belser, M. Stöhr, A. Pfaltz, *J. Am. Chem. Soc.* **2005**, *127*, 8720.

[39] a) M. T. Cuberes, R. R. Schlittler, J. K. Gimzewski, Appl. Phys. A 1998, 66, S669; b) T. Kamikado, T. Sekiguchi, S. Yokoyama, Y. Wakayama, S. Mashiko, *Thin Solid Films* **2006**, *499*, 329.

[40] S. Berner, M. de Wild, L. Ramoino, S. Ivan, A. Baratoff, H. J. Güntherodt, H. Suzuki, D. Schlettwein, T. A. Jung, *Phys. Rev. B* **2003**, *68*, 115410.

[41] The model is derived from Spartan calculations (Spartan'06, Wavefunction, Inc., Irvine, CA.). Approximate arrangements of the two interacting porphyrins were taken from the surface data and simulated in the gas phase using both PM3 and AM1 methods.

[42] Y. Okuno, T. Yokoyama, S. Yokoyama, T. Kamikado, S. Mashiko, *J. Am. Chem. Soc.* **2002**, *124*, 7218.

[43] M. Itoh, M. Takamatsu, N. Kizu, Y. Fujiwara, *J. Phys. Chem.* **1991**, *95*, 9682.

[44] T. Michinobu, C. Boudon, J. P. Gisselbrecht, P. Seiler, B. Frank, N. N. P. Moonen, M. Gross, F. Diederich, *Chem. Eur. J.* **2006**, *12*, 1889.

[45] F. Tao, S. L. Bernasek, *J. Am. Chem. Soc.* **2005**, *127*, 12750.

[46] M. J. Crossley, L. D. Field, A. J. Forster, M. M. Harding, S. Sternhell, *J. Am. Chem. Soc.* **1987**, *109*, 341.

[47] M. Böhringer, W. D. Schneider, R. Berndt, *Angew. Chem.* **2000**, *112*, 821; *Angew. Chem. Int. Ed.* **2000**, *39*, 792.

[48] a) D. S. Reddy, B. S. Goud, K. Panneerselvam, G. R. Desiraju, *J. Chem. Soc. Chem. Comm.* **1993**, *663*; b) D. Britton, *J. Chem. Crystallogr.* **1991**, *27*, 405; c) U. Drück, A. Kutoglu, *Acta Crystallogr. C* **1983**, *39*, 638.

[49] S. De Feyter, F. C. De Schryver, *Chem. Soc. Rev.* **2003**, *32*, 139.

[50] G. M. Whitesides, J. P. Mathias, C. T. Seto, *Science* **1991**, *254*, 1312.

[51] L. Wang, D. Qi, L. Liu, S. Chen, X. Gao, A. T. S. Wee, *J. Phys. Chem. C* **2007**, *111*, 3454.

[52] L. Gross, K. H. Rieder, A. Gourdon, C. Joachim, F. Moresco, *ChemPhysChem* **2007**, *8*, 245.

[53] L. Merz, H. Güntherodt, L. J. Scherer, E. C. Constable, C. E. Housecroft, M. Neuburger, B. A. Hermann, *Chem. Eur. J.* **2005**, *11*, 2307.

[54] K. K. Frederick, M. S. Marlow, K. G. Valentine, A. J. Wand, *Nature* **2007**, *448*, 325; R. S. Spolar, M. T. Record, *Science* **1994**, *263*, 777.

[55] J. M. Sturtevant, *P. Natl Acad. Sci. USA* **1977**, *74*, 2236.

[56] a) C. H. Lee, J. S. Lindsey, *Tetrahedron* **1994**, *50*, 11427; B. J. Littler, Y. Ciringh, J. S. Lindsey, *J. Org. Chem.* **1999**, *64*, 2864; b) L. H. Yu, J. S. Lindsey, *J. Org. Chem.* **2001**, *66*, 7402.

[57] S. Buchholz, J. P. Rabe, *J. Vac. Sci. Technol. B* **1991**, *9*, 1126.

[58] see "www.kentax.de"

3.1.2 Discussion

In the presented article it has been shown that the possibilities to control the self-assembly process can be greatly enhanced by transfering the concept of synthons which is well known from supramolecular chemistry into the field of supramolecular surface assemblies. We have concentrated on the influence of different alkoxyphenyl side-groups which have been attached to the same molecular core, on the resulting 2D structure, while in previous work by other groups, mainly the whole molecular structure was changed which lead to different assemblies.[53, 54]

First we have shown that, depending on the steric demand of the chosen alkoxyphenyl substituents, the assembly can be forced either into a one- or a two-dimensional phase. In the context of miniaturization, self-assembled one-dimensional wires are of highest importance for the transmission of signals and currents. Unfortunately, no suitable possibility to connect an existing macro-circuit to a molecular wire has been found so far. The presented work offers a new level of control over the self-assembles structures and even provides a method to create wires and supramolecular devices out of the same molecular compounds. This method by which different synthons are combined and which makes use of their different steric demands goes far beyond what has been achieved so far in addressable supramolecular structures.

Furthermore, we have demonstrated that by skillfully choosing the molecular substituents the properties of the two-dimensional assemblies can be altered in a controlled way. Specifically, we have shown that the porphyrin building block together with the cyanophenyl synthon in opposing positions is mainly responsible for the formation of nanoporous networks on a Cu(111) surface. By using different alkoxyphenyl substituents for the remaining two positions at the porphyrin core, one parameter of these networks, namely the pore-to-pore distance, was changed in a controlled way. This phenomenon was attributed to the steric demand of the substituents together with the balancing of the entropic losses of the different alkoxy chains by van-der-Waals interactions. The latter is a very important factor in every kind of self-assembled structure (see section 2.5) and thus a detailed understanding of the involved mechanisms is crucial for gaining control over the self-assembly process.

The ability to control the properties of nanoporous networks is of high importance due to the variety of possible technological applications connected to them. Due to the porous structure, they might be used as specific sensors which are capable to host distinct types of molecules or, in comparison to the function of some proteins in cell membranes, as channels for specific molecules. Due to the regular, two-dimensional arrangement, the pores of a

nanoporous network can be individually addressed. This, together with their capabillity to host different guest molecules,[46, 55] makes them ideal candidates for memory devices. As the guest molecules can change the properties of the hosting network[55] they could be used as detection systems capable of distinguishing between different species.

For adapting the nanoporous networks to the different needs of the aforementioned applications, it is necessary to be able to precisely control their properties. One example how to achieve this goal, the change of the pore-to-pore distance, is given in the presented article. The second important parameter in nanoporous networks is the pore diameter. However, to change this requires to completely redesign the molecular substituents including the cyanophenyl synthon. The synthesis of a new porphyrin derivative with appropriate substituents to achieve this goal is currently being done by Jens Hornung of the ETH Zürich.

3.2 A Supramolecular Device Formed by P4

The following is a copy of the article published in *Angewandte Chemie*. Please note that the porphyrin derivative **P4** is called molecule **1** in this publication.

3.2.1 Publication B

Molecular Devices

DOI: 10.1002/ange.200700285

A Supramolecular Multiposition Rotary Device**

Nikolai Wintjes, Davide Bonifazi, Fuyong Cheng, Andreas Kiebele, Meike Stöhr, Thomas Jung, Hannes Spillmann,* and François Diederich**

In recent years, artificial molecular devices have been strongly in the focus of research.[1] Bi- or multistable molecules as well as supramolecular assemblies have been built using highly sophisticated strategies.[2] Triggered by external stimuli, electronic and conformational states of these systems can be reversibly switched.[3] While the majority of these strategies result in large thermodynamic ensembles supported within fluids or the 3D bulk, recent advances allow for the deposition of complex units onto solid surfaces.[4] Thereby, reversible conformational changes and isomerizations of single molecules can be induced with local probe techniques such as scanning tunneling microscopy (STM) or atomic force microscopy (AFM).[5] Also, systems are known in which the adsorption state or site of a whole molecule is changed; this happens either thermally[6] or can be induced by the STM tip.[7] For technological applications, however, it is highly important to place supramolecular devices in an ordered and easily accessible structure such as a two-dimensional lattice.

Herein, we show that highly complex and ordered supramolecular entities can be fabricated on solid surfaces by taking advantage of a self-organization process, which follows the self-assembly approach introduced by Lehn.[8] Specifically, self-assembly of a specially functionalized porphyrin molecule (Figure 1) leads on Cu(111) surfaces to the formation of a regular nanoporous network that hosts single porphyrin guests nested on top of the pores. This unprecedented structural arrangement allows the guest to rotate. Because it is not placed directly on the surface, as in other existing rotational systems on metals,[9] it can snap into six different positions, of which three are distinguishable by the STM technique. Ultimately, the regular arrangement leads to the possibility of independently addressing each entity by labeling its position within the network and determining its state by looking at the arrangement of the guest relative to the STM scanning direction.

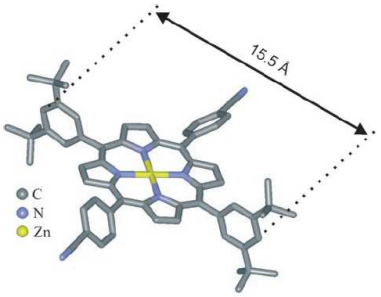

Figure 1. Optimized molecular structure of the porphyrin derivative **1**[21] used in this study, as generated by PM3 calculations implemented within Spartan.

Porphyrin **1** was vapor-deposited under ultrahigh vacuum (UHV) conditions on an atomically clean and flat Cu(111) surface. In the submonolayer regime the porphyrin molecules self-assemble into a highly ordered two-dimensional porous network (Figure 2a) with a pore–pore distance of (32 ± 1) Å and a pore diameter of (18 ± 1) Å (measured as indicated by the yellow circle in Figure 2a), as determined by the analysis of several STM images at variable temperatures (between 77 K and 298 K).[10] In the STM images each pore appears as a chiral windmill-shaped structure consisting of six wings. Each wing itself can be resolved by high-resolution imaging into two separated lobes, of which the outer one usually appears brighter. For the arrangement of the porous network, two homochiral domains are possible[11] in which the wings are organized either clockwise or counterclockwise (Figure 2b). The two lobes that form the windmill structure can be associated with the two *tert*-butyl residues contained in the 3,5-di(*tert*-butyl)phenyl substituents.[12] The less bright structures between two parallel wings (Figure 2c) can be attrib-

[*] Dr. T. Jung
Laboratory for Micro- and Nanotechnology
Paul Scherrer Institute
5232 Villigen PSI (Switzerland)
Fax: (+41) 56-310-2646
E-mail: thomas.jung@psi.ch
Homepage: http://monet.unibas.ch/gue/nanolab/publications/publications.htm

N. Wintjes, Dr. A. Kiebele, Dr. M. Stöhr, Dr. H. Spillmann
Institute of Physics
University of Basel
4056 Basel (Switzerland)
Fax: (+41) 61-267-3784
E-mail: h.spillmann@unibas.ch

Dr. D. Bonifazi, Dr. F. Cheng, Prof. Dr. F. Diederich
Laboratorium für Organische Chemie
ETH-Zürich
Hönggerberg, HCI, 8093 Zürich (Switzerland)
Fax: (+41) 44-632-1109
E-mail: diederich@org.chem.ethz.ch

[**] This work was supported by the Swiss National Science Foundation, the NCCR "Nanoscale Science", and the European Union through the Marie Curie Research Training Network PRAIRIES (MRTN-CT-2006-035810). We thank the Swiss Federal Commission for Technology and Innovation, KTI, and Nanonis Inc. for the fruitful collaboration on the data-acquisition system.

Supporting information for this article is available on the WWW under http://www.angewandte.org or from the author.

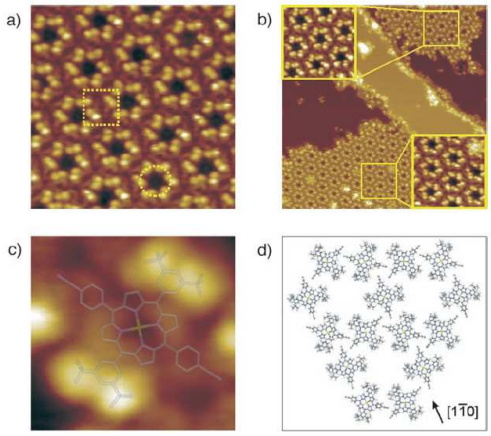

Figure 2. STM images taken with $U_{gap} = -1.5$ V, $I_{tunnel} = 20$ pA, and a sample coverage around 20%. a) STM image (scan range: 12.5×12.5 nm^2) of a self-assembled network of porphyrin **1** on an atomically clean Cu(111) surface. The dashed rectangle marks the position where the image in Figure 2c was taken. b) The network can be found in two homochiral domains (scan range: 50×50 nm^2; insets: 9.1×9.1 nm^2). c) Detailed view of a single molecule inside the porphyrin network (scan range: 2.1×2.1 nm^2). A transparent model of porphyrin **1** is embedded to show the location of the molecule and the structure–image correlation. d) Proposed pattern model of the two-dimensional porous network.

uted to the central tetrapyrrolic core and to the 4-cyanophenyl groups.[13] Therefore, a single molecule in the network can be identified as a rectangle with bright lobes on the edges and mean dimensions of 4.0 Å and 14.7 Å for the smaller and longer sides, respectively. These distances reflect very well the intramolecular distances (approximately 5.0 Å and 15.5 Å) as measured from the PM3-optimized geometry of porphyrin **1**.

On the basis of this structural correlation, we were able to develop a model of the porous network (Figure 2d; see Movie 3 in the Supporting Information). According to this proposed pattern, each nanopore is surrounded by six flat-lying porphyrins whereas each porphyrin is part of two neighboring pores. Based on the fact that in STM images each 3,5-di(*tert*-butyl)phenyl substituent appears as a brighter and a darker lobe, by comparison with previous studies of similar porphyrins deposited on Au(111) and Cu(111) surfaces,[13,14] the dihedral angle between the 3,5-di(*tert*-butyl)phenyl substituents and the porphyrin core is estimated to be about 20°. Furthermore, in the proposed model each 4-cyanophenyl group points towards the hydrogen atoms of a 4-cyanophenyl group of a neighboring porphyrin molecule. We therefore believe that the formation of the network is likely driven by weak hydrogen-bonding interactions between the phenyl rings and the cyano residues, as it has been reported for supramolecular aggregates and porous networks of similar porphyrins.[15]

Parallel to the self-assembly of the porous network, we have found that at a temperature of 77 K some of the pores are occupied by a four-lobed structure that appears much brighter in the STM images than the empty pore (Figure 3a). As we added no other types of molecules, the only explanation for this observation is self-trapping of porphyrin **1**. The lobes form a rectangle with mean dimentions of 3.4 Å and

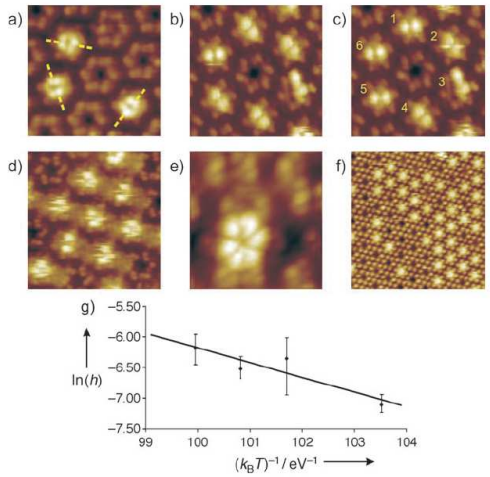

Figure 3. a–f) STM images of the porphyrin network taken with $U_{gap} = -1.5$ V, $I_{tunnel} = 20$ pA, and a sample coverage around 10% (a–c) or around 30–40% (d–f) at different temperatures (from 77 K to 298 K). Some of the pores are filled. a) At 77 K the filling of the pore can be resolved into four rectangularly arranged lobes (scan range: 10.2×10.2 nm^2). These can take three distinguishable positions, all of which occur in the imaged frame (as indicated by the dashed lines). b,c) At 112 K only two lobes are visible (scan range: 7.4×7.4 nm^2). They can switch to a different position over time (see especially structures 1 and 5). d) At 115 K the porphyrin guest appears extremely fuzzy (scan range: 8.8×8.8 nm^2). e) At 150 K all possible positions can be seen simultaneously leading to a flowerlike appearance of the pore filling (scan range: 3.0×3.0 nm^2). f) At room temperature some pores seem to be completely filled (scan range: 29.9×29.9 nm^2). g) Arrhenius plot for the determination of the activation energy needed to switch between two neighboring positions.[22]

8.1 Å for the smaller and longer sides, respectively. This structure shows a striking similarity to the appearance of a single porphyrin molecule in the network (Figure 2c), although the mean length of the longer sides is almost 45% smaller. Nevertheless, Moresco et al.[14] and also Sekiguchi et al.[16] have observed that for similar molecules the intramolecular distances can appear drastically reduced in STM images as a result of conformational changes of the 3,5-di(*tert*-butyl)phenyl substituents. We assume that a similar mechanism takes place here and therefore conclude that the lobes belong to one single porphyrin molecule nested horizontally on top of a pore (see also the Supporting Information). As the supporting pore has a hexagonal symmetry, the porphyrin guest molecule can take six different positions separated by a rotational angle of 60°. Because of the structural guest symmetry (C_{2h}), only three of these positions are distinguishable. In Figure 3a, three porphyrin guests, arranged in one of the three distinguishable positions, are shown.

After the sample is heated to 112 K, the guest molecules appear mostly as two opposing lobes (Figure 3b and c). This behavior might be a result of a thermally induced shivering of the 3,5-di(*tert*-butyl)phenyl groups. Very interestingly, in STM sequences we discovered that the guest molecules can thermally switch from one stable position to another (Movie 1 in the Supporting Information). Figure 3b and c show two subsequent STM images (148 seconds per image). One can clearly see that the porphyrin guests 1 and 5 in Figure 3c have switched. The horizontal line in pore 2 indicates that the nested molecule switched into a new position and then back while scanning the underlying pore. A preferred rotational direction or hopping to neighboring pores[17] was never observed. Molecule 3 seems to be adsorbed onto a position which prevents the rotation. Such defects are observed only very rarely.

At a temperature of 115 K the structure of the porphyrin guest appears extremely fuzzy (Figure 3d, see also Movie 2 in the Supporting Information), and at 150 K the fillings show a flowerlike structure consisting of six leaves (Figure 3e). This observation can be explained by the characteristic scanning speed of the STM in the millisecond range for each imaged pixel. At elevated temperatures, the thermally induced rotation of the nested molecules is faster than the time resolution of the STM. Thus, the molecules change their position while the STM tip is scanning across them and give rise to fuzzy imaging. Above a certain rotational speed, the STM image shows a superposition of all possible positions that the guest molecule can take on a single pore, leading to the shown flowerlike structure.[18] At room temperature, even this structure disappears and owing to the very high rotational speed of the nested molecule the pores appear completely filled (Figure 3f).

From the analysis of successive STM images taken at temperatures between 112 K and 116 K, we estimated the switching activation energy by applying a model that is commonly used to describe the diffusion of molecules on metal surfaces.[19] By counting the number of guests that did not switch in the time interval between two STM frames, we obtained the switching rate h. From the Arrhenius plots of h versus $(k_B T)^{-1}$ (Figure 3g), we then extrapolated an activation energy of (0.24 ± 0.08) eV with a pre-exponentional constant of around $5 \times 10^7\ s^{-1}$ (standard deviation $= \pm 1 \times 10^{2.8}\ s^{-1}$). Nevertheless, owing to the characteristic scanning speed of the STM, the activation energy determined by this method is slightly underestimated.[20]

As the guest molecule is embedded into a nanoporous network, each device can be selectively addressed and switched by the STM tip. For this purpose the sample was cooled down to a temperature where no thermally induced switching occurs ($T = 77$ K). The tip was then placed above a porphyrin guest under scanning conditions ($U_{gap} = -1.5$ V, $I_{tunnel} = 10$ pA). By applying short pulses (around 1 s) with $U_{gap} = -0.7$ V and $I_{tunnel} = 150$ pA, single switching events could be triggered. Figure 4a and b show one typical example where tip-induced switching was applied to the porphyrin guest in the right part of the image. One can clearly see that the guest switched into a different position, while the neighboring one (on the left) did not rotate. Although this method revealed to be successful in inducing a switching event, the direction of rotation (i.e., clockwise or counterclockwise) could not be preferentially induced.

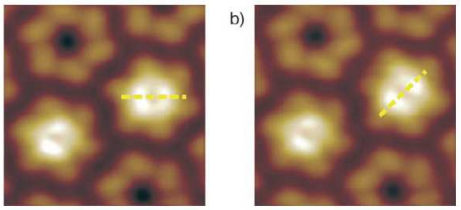

Figure 4. Controlled rotation of the nested guest molecules can be induced by the STM tip. a, b) STM images recorded with a scan range of 6.5×6.5 nm^2, $U_{gap} = -1.5$ V, and $I_{tunnel} = 10$ pA. The guest on the right in part (a) was switched by applying a short pulse with $I_{tunnel} = 150$ pA at $U_{gap} = -0.7$ V.

In conclusion, we have demonstrated that by skillful functionalization, organic molecules can self-assemble into complex and independently addressable supramolecular nanodevices. Future refinements of the approach presented here may provide assemblies with activation energies that are high enough for technologic applications.

Received: January 22, 2007
Revised: February 26, 2007
Published online: April 20, 2007

Keywords: copper · porphyrinoids · scanning probe microscopy · self-assembly · supramolecular chemistry

[1] a) M. Irie, *Chem. Rev.* **2000**, *100*, 1685–1716; b) Special Issue on Molecular Machines: *Acc. Chem. Res.* **2001**, *34*(6); c) G. S. Kottas, L. I. Clarke, D. Horinek, J. Michl, *Chem. Rev.* **2005**, *105*, 1281–1376.

[2] a) E. R. Kay, D. A. Leigh, F. Zerbetto, *Angew. Chem.* **2007**, *119*, 72–196; *Angew. Chem. Int. Ed.* **2007**, *46*, 72–191; b) D. Sato, T. Akutagawa, S. Takeda, S.-I. Noro, T. Nakamura, *Inorg. Chem.* **2007**, *46*, 363–365.

[3] a) S. P. Fletcher, F. Dumur, M. M. Pollard, B. L. Feringa, *Science* **2005**, *310*, 80–82; b) M. C. Jiménez, C. Dietrich-Buchecker, J.-P. Sauvage, *Angew. Chem.* **2000**, *112*, 3422–3425; *Angew. Chem. Int. Ed.* **2000**, *39*, 3284–3287; c) T. Hugel, N. B. Holland, A. Cattani, L. Moroder, M. Seitz, H. E. Gaub, *Science* **2002**, *296*, 1103–1106; d) J. D. Badjić, V. Balzani, A. Credi, S. Silvi, J. F. Stoddart, *Science* **2004**, *303*, 1845–1849; e) D. W. Steuerman, H. R. Tseng, A. J. Peters, A. H. Flood, J. O. Jeppesen, K. A. Nielsen, J. F. Stoddart, J. R. Heath, *Angew. Chem.* **2004**, *116*, 6648–6653; *Angew. Chem. Int. Ed.* **2004**, *43*, 6486–6491; f) H. Kanazawa, M. Higuchi, K. Yamamoto, *J. Am. Chem. Soc.* **2005**, *127*, 16404–16405; g) V. A. Azov, A. Schlegel, F. Diederich, *Angew. Chem.* **2005**, *117*, 4711–4715; *Angew. Chem. Int. Ed.* **2005**, *44*, 4635–4638; h) J. Berná, D. A. Leigh, M. Lubomska, S. M. Mendoza, E. M. Pérez, P. Rudolf, G. Teobaldi, F. Zerbetto, *Nat. Mater.* **2005**, *4*, 704–710.

[4] a) T. Ye, T. Takami, R. Wang, J. Jiang, P. S. Weiss, *J. Am. Chem. Soc.* **2006**, *128*, 10984–10985; b) J. Otsuki, S. Shimizu, M. Fumino, *Langmuir* **2006**, *22*, 6056–6059; c) L. Scudiero, D. E. Barlow, U. Mazur, K. W. Hipps, *J. Am. Chem. Soc.* **2001**, *123*, 4073–4080.

[5] a) F. Moresco, G. Meyer, K. H. Rieder, H. Tang, A. Gourdon, C. Joachim, *Phys. Rev. Lett.* **2001**, *86*, 672 – 675; b) H. Yanagi, K. Ikuta, H. Mukai, T. Shibutani, *Nano Lett.* **2002**, *2*, 951 – 955; c) C. Loppacher, M. Guggisberg, O. Pfeiffer, E. Meyer, M. Bammerlin, R. Luthi, R. R. Schlittler, J. K. Gimzewski, H. Tang, C. Joachim, *Phys. Rev. Lett.* **2003**, *90*, 066107; d) J. Henzl, M. Mehlhorn, H. Gawronski, K.-H. Rieder, K. Morgenstern, *Angew. Chem.* **2006**, *118*, 617 – 621; *Angew. Chem. Int. Ed.* **2006**, *45*, 603 – 606; e) M. Alemani, M. V. Peters, S. Hecht, K.-H. Rieder, F. Moresco, L. Grill, *J. Am. Chem. Soc.* **2006**, *128*, 14446 – 14447.

[6] a) O. P. H. Vaughan, F. J. Williams, N. Bampos, R. M. Lambert, *Angew. Chem.* **2006**, *118*, 3863 – 3865; *Angew. Chem. Int. Ed.* **2006**, *45*, 3779 – 3781; b) S. Weigelt, C. Busse, L. Petersen, E. Rauls, B. Hammer, K. V. Gothelf, F. Besenbacher, T. R. Linderoth, *Nat. Mater.* **2006**, *5*, 112 – 117.

[7] a) P. A. Lewis, Ch. E. Inman, F. Maya, J. M. Tour, J. E. Hutchison, P. S. Weiss, *J. Am. Chem. Soc.* **2005**, *127*, 17421 – 17426; b) J. A. Heinrich, C. P. Lutz, J. A. Gupta, D. M. Eigler, *Science* **2002**, *298*, 1381 – 1387; c) L. J. Lauhon, W. Ho, *J. Chem. Phys.* **1999**, *111*, 5633 – 5636; d) F. Chiaravalloti, L. Gross, K.-H. Rieder, S. Stojkovic, A. Gourdon, C. Joachim, F. Moresco, *Nat. Mater.* **2007**, *6*, 30 – 33.

[8] J.-M. Lehn, *Supramolecular Chemistry*, VCH, Weinheim, **1995**.

[9] J. K. Gimzewski, C. Joachim, R. R. Schlittler, V. Langlais, H. Tang, I. Johannsen, *Science* **1998**, *281*, 531 – 533.

[10] The temperature is measured in close proximity to the sample in thermal contact.

[11] S. De Feyter, F. C. De Schryver, *Chem. Soc. Rev.* **2003**, *32*, 139 – 150.

[12] T. A. Jung, R. R. Schlitter, J. K. Gimzewski, H. Tang, C. Joachim, *Science* **1996**, *271*, 181 – 184.

[13] T. Yokoyama, S. Yokoyama, T. Kamikado, Y. Okuno, S. Mashiko, *Nature* **2001**, *413*, 619 – 621.

[14] F. Moresco, G. Meyer, K. H. Rieder, H. Ping, H. Tang, C. Joachim, *Surf. Sci.* **2002**, *499*, 94 – 102.

[15] a) Y. Okuno, T. Yokoyama, S. Yokoyama, T. Kamikado, S. Mashiko, *J. Am. Chem. Soc.* **2001**, *123*, 7218 – 7225; b) H. Spillmann, A. Kiebele, M. Stöhr, T. A. Jung, D. Bonifazi, F. Y. Cheng, F. Diederich, *Adv. Mater.* **2006**, *18*, 275 – 279; c) D. Bonifazi, A. Kiebele, M. Stöhr, F. Y. Cheng, T. Jung, F. Diederich, H. Spillmann, *Adv. Funct. Mater.* **2007**, in press.

[16] T. Sekiguchi, Y. Wakayama, S. Yokoyama, T. Kamikado, S. Mashiko, *Thin Solid Films* **2004**, *464–465*, 393 – 397.

[17] a) A. Kiebele, D. Bonifazi, F. Cheng, M. Stöhr, F. Diederich, T. Jung, H. Spillmann, *ChemPhysChem* **2006**, *7*, 1462 – 1470; b) G. Schull, L. Douillard, C. Fiorini-Debuisschert, F. Charra, F. Mathevet, D. Kreher, A.-J. Attias, *Adv. Mater.* **2006**, *18*, 2954 – 2957.

[18] M. Stöhr, Th. Wagner, M. Gabriel, B. Weyers, R. Möller, *Phys. Rev. B* **2001**, *65*, 033404.

[19] B. G. Briner, M. Doering, H.-P. Rust, A. M. Bradshaw, *Science* **1997**, *278*, 257 – 260.

[20] M. Schunack, T. R. Linderoth, F. Rosei, E. Laegsgaard, I. Stensgaard, F. Besenbacher, *Phys. Rev. Lett.* **2002**, *88*, 156102.

[21] F. Cheng, S. Zhang, A. Adronov, L. Echegoyen, F. Diederich, *Chem. Eur. J.* **2006**, *12*, 6062 – 6070.

[22] The relatively large error bar at $(k_B T)^{-1} = 101.70\ eV^{-1}$ originates from the fuzzy imaging of the molecules at this temperature (see main text), which makes it difficult to decide whether a nested molecule changed its position or not.

3.2.2 Discussion

In the presented article the supramolecular self-assembly which resulted out of a small change in the molecular structure of the porphyrin derivatives used in section 3.1 has been described. The flexible alkoxy chains which were exploited to control the pore-to-pore distance in the first publication have been exchanged by bulky *tert*-butyl groups. The cyanophenyl substituent which has been shown to be mainly responsible for the formation of the porous network, has not been changed. Thus, the molecules self-assemble into a nanoporous network similar to the ones presented in the first publication. However, as the *tert*-butyl groups which form the rim of a pore are rigid and exhibit primarily rotational degrees of freedom, also the rim itself is, in contrast to the pores in the networks presented in section 3.1.1, rigid and thus well-defined. This leads to the possibility of nesting porphyrin guest molecules on top of the pores, presumably due to an interaction between the *tert*-butyl groups of the nested molecules and those of the molecules inside the network. This arrangement is only possible due to a delicate relation between the pore diameter and the size of the nested guest molecules. Because of the symmetry of the system, the nested molecules are found in three distinguishable positions. By thermal activation or interactions with the tip, they can hop between these positions without disrupting the entity or hopping to a neighboring pore.

One of the main goals in nanotechnology is mimicking the functions of existing devices, as transistors, wires, or switches. For technological applications it is furthermore desirable to be able to produce a large number of devices in a fast and reproducible way. In the presented publication, an example of a fully self-assembled device is presented. It proves that by using organic molecules as building blocks for complicated assemblies the aforementioned goals can be achieved. However, the presented device has still some draw-backs. First, the temperature of operation is too low. For the use as a technological application, this temperature must be increased to make the device operational at room temperature. This might be possible by increasing the interaction of the nested porphyrin molecule with the supporting substrate which should also increase the interaction energy required for a hopping to take place. This can be reached for example by increasing the pore diameter and thereby also the bending of the nested porphyrin towards the substrate. However, this requires to completely redesign the molecule with altered side-groups. The synthesis of a new porphyrin derivative to achieve this goal is currently being done by Jens Hornung at the ETH Zürich. Second, the direction of rotation for the nested molecule cannot be predicted. At current, the rotation is induced by heating the system. Also

the tip induced rotation of an individual nested guest is in principle done by locally induced heat. However, heating is an undirected process and thus will not lead to a preferred rotational direction. Also the chirality of the underlying network cannot be exploited to guide the direction of heat induced rotations, as, unlike in the macroscopic world, on the atomic or molecular scale, directing a rotation by potential barriers with different slopes is not possible.[56] Therefore, our current studies are taking into account also magnetic and chemical approaches. One possibility might be to design the supporting porous network and the nested molecules out of two different types of molecules, whereas the nested guest molecule provides magnetic properties. Some knowledge in the field of hosting guest molecules of different types was recently gained by our group.[45, 46, 55]

3.3 Bimolecular Systems

In the following, two studies on bimolecular systems are presented. Depending on their ability to mutually compensate for the occuring loss of entropy, as described in section 3.1, the two systems show different behaviors: The first system exhibits separated phases while the second system self-assembles into an intermixed network consisting of both molecular compounds. Together, these two systems illustrate nicely the importance of considering the entropy in molecular self-assembly.

3.3.1 Separated Phases of P3 and P4

In the first study, we evaporated the two very similar porphyrin derivatives **P3** and **P4** (see section 2.4.2) onto a Cu(111) surface. They differ only in the type of the alkyl substituents. While **P3** has four flexible isopentoxy chains, with many degrees of conformational freedom, the *tert*-butyl groups of **P4** are rigid and their conformational degree of freedom is mainly attributed to a rotation of the tertiary butyl groups around the phenyl-carbon bond.

The behavior of **P3** and **P4** on the Cu(111) surface has been described in detail in sections 3.1 and 3.2. In a successive experiment, we evaporated both derivatives subsequently onto a freshly cleaned Cu(111) surface. This results in a separation of the two compounds into two phases (Figure 3.5). **P3** forms the molecular chains described in section 3.1.1 for corresponding coverages and **P4** forms the network presented in section 3.2.1. A mixed network consisting of **P3** and **P4** molecules has not been found. However, the molecular chains formed by **P3** often start at the borders of the network formed by **P4**. This behavior can be easily explained by anti-parallel dipole-dipole interactions of the cyano groups which both derivatives exhibit, similar to the mechanism described in section 3.1.1 for the formation of the molecular chains of **P3**. The **P4** molecules at the border of the network act as additional nucleation sites for the molecular chains of **P3**, similar to the molecules covering the step edges, as described in the same section. Upon increasing the coverage of **P3**, the molecules form the network known from section 3.1.1. Also then, an intermixing of the molecules was not observed.

The absence of an intermixed network of the two molecular species can be understood by taking into acount the characteristics of the different side-groups of the two molecules. When the flexible diisopentoxy chains of **P3** are confined inside a network, they are restricted in their mobility, as shown in section 3.1.1. The according loss of entropy must be compensated by increased intermolecular interactions. This can be done more efficient by an interaction with another diisopentoxy chain than with the bulky *tert*-butyl

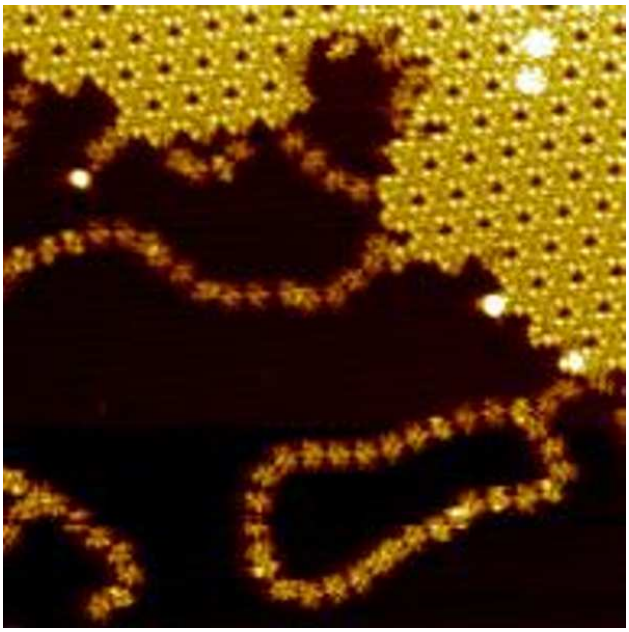

Figure 3.5: The subsequent evaporation of the porphyrin derivatives **P3** and **P4** resulted in the formation of two phases, each one being formed by only one of the molecular species (Image taken with $U_{\text{gap}} = -2.0$ V, $I_{\text{tunnel}} = 15$ pA, scan range: 50×50 nm^2). The phases resemble those formed after evaporating only one species onto a clean Cu(111) surface at the corresponding coverages (Figure 3.2 in the first publication, section 3.1 and Figure 2 in the second publication, section 3.2).

groups. Thus, no intermixed network of the two molecular species occurs. The anti-parallel dipole-dipole interaction, however, is possible, because the 4-cyanophenyl group is not flexible like the alkoxy chains of **P3** and does not need significant entropic compensation to reduce translational movements. Interestingly, almost no **P4** molecules are found inside the molecular chains. This can be explained by the fact that the trimeric arrangement is energetically more profitable for the unhindered cyano group, as stated in section 3.1.1.

The system shows nicely the need for compensation of the entropic term. Although both derivatives are very closely related, exhibit basically the same atomical structure, and can self-assemble into very similar networks, they do not form a mixed network consisting of both derivatives, because the *tert*-butyl groups of **P4** cannot compensate for the entropic losses of the alkoxy chains of **P3** as effectively as another alkoxy chain.

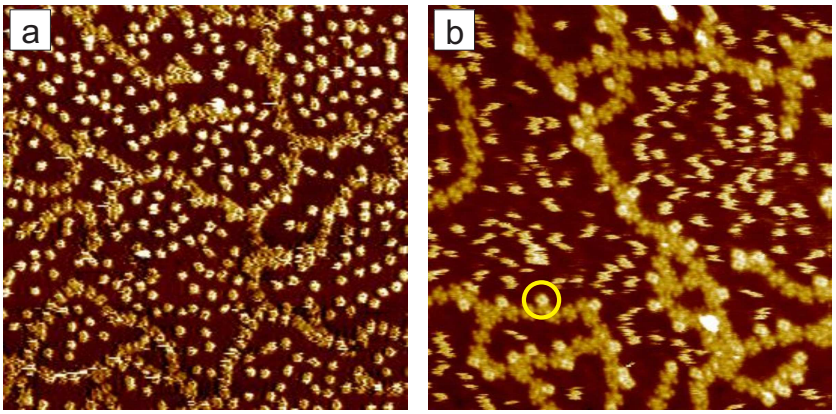

Figure 3.6: STM images showing the result of subsequent evaporation of 0.15 ML of **P3** and 0.05 ML of ZnOEP on a Cu(111) surface. a) At a temperature of 77 K the **P3** molecules are ordered in the chain phase known from section 3.1, whereas the ZnOEP molecules are randomly distributed on the surface ($U_{\text{gap}} = -1.7$ V, $I_{\text{tunnel}} = 20$ pA, scan range: 70×70 nm^2). They do not show lateral diffusion. b) At a temperature of 85 K the ZnOEP molecules exhibit slow lateral diffusion ($U_{\text{gap}} = -1.5$ V, $I_{\text{tunnel}} = 20$ pA, scan range: 50×50 nm^2). Some ZnOEP molecules however are firmly attached to the **P3** chains (yellow circle) and do not exhibit any mobility.

3.3.2 A Mixed Network Formed by P3 and ZnOEP

After discussing the reason why the two derivatives **P3** and **P4** did not self-assemble into a mixed phase (section 3.3.1), we altered the experiment in a way that, according to the knowledge gained in the previous sections, should allow for an intermixing of the used molecular species. We exchanged the derivative **P4**, which only consists of rigid moieties, with the derivative **ZnOEP** (2.4.3), which has eight short but flexible alkyl chains. Because of their higher number of conformational degrees of freedom compared to the *tert*-butyl groups, they should be potentially able to interact with the isopentoxy chains of **P3** via van-der-Waals forces and thereby compensate for the loss of entropy of these moieties.

We subsequently evaporated 0.15 ML of **P3** and 0.05 ML of **ZnOEP** on a Cu(111) surface and cooled the system down to a temperature of 77 K. By this, **P3** self-assembled into the chain phase described in sections 3.1 and 3.3.1, while the **ZnOEP** molecules were spread statistically on the remaining parts of the surface (Figure 3.6a). This surprising result indicates that the intermolecular interactions between the **ZnOEP** molecules must be

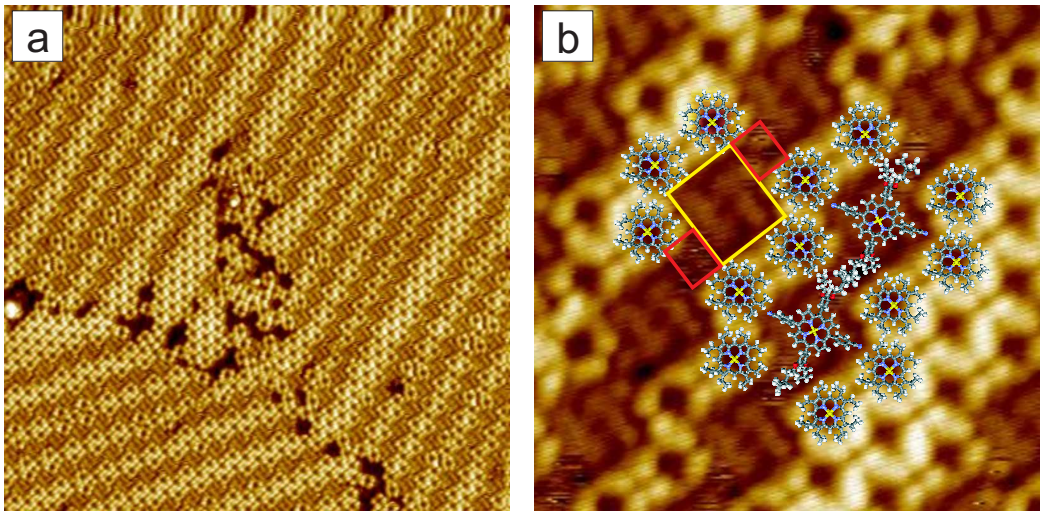

Figure 3.7: a) After subsequent evaporation of 0.15 ML of **P3** and 0.70 ML of **ZnOEP**, the molecules self-assemble into a mixed network consisting of both derivatives (scan range: 50×50 nm^2). The two molecular species can be easily distinguished by their appearance and apparent height (i.e. the brightness) in the STM image. b) STM image (15×15 nm^2) providing a detailed view of the network. Molecular models have been overlaid to show the locations of the molecules. The yellow rectangle marks one cavity in which the core and the cyanophenyl substituents of **P3** are nested and the red rectangles mark the areas which are interconneting two cavities and in which the alkoxyphenyl substituents are situated. Both STM images were taken with $U_{\text{gap}} = -1.1$ V, $I_{\text{tunnel}} = 10$ pA at a temperature of 77 K.

very low or even repulsive[55] at this coverage. We then heated the sample to a temperature of 85 K, at which the **ZnOEP** molecules exhibit a very slow diffusion on the Cu(111) surface (Figure 3.6b). This is evident from STM images in which the molecules appear to leave a short trail and cannot be clearly resolved anymore. However, some **ZnOEP** molecules are found attached to the **P3** chains where they do not exhibit any mobility at all (yellow circle in Figure 3.6b). As no multimeres of **ZnOEP** molecules are found on the bare copper surface, this result indicates that an interaction between **ZnOEP** and **P3** is stronger than one between only **ZnOEP** molecules.

After increasing the coverage of **ZnOEP** to 0.7 ML, the chains formed by **P3** diappeared. Instead, the two derivatives self-assembled into a mixed network consisting of both derivatives (Figure 3.7a). Inside the network, the discrimination of the two molecular compounds is easily possible. The

appearance of the **ZnOEP** molecules resembles the one of CuOEP molecules described in Ref.[21] at the applied voltages. The CuOEP molecule has the same structure as **ZnOEP** and differs only in the central ion which does not have an influence on the resulting self-assembly as shown by Hipps *et al.* for phthalocyanines[57] and is also evident by comparing the assemblies reported in Ref.[21] with the network presented here. The **ZnOEP** molecules have a rectangular shape with bright sides which can be attributed to the ethyl chains and a dark interior which resembles the porphyrin ring. The signal derived from the **P3** molecules is much weaker in comparison and thus the molecules appear darker in the STM images. The appearance of an individual **P3** molecule equals that described in section 3.1 (compare Figure 3.1a). As a common feature, streaks are caused by mobile alkoxy chains and thus hint to their location in the network.

The intermixed network consists of alternating rows of the two derivatives. As a response to the threefold symmetry of the surface, these rows can be found along three different directions (two of them are shown in Figure 3.7a). Due to the excess of **ZnOEP** molecules on the surface, the lines formed by this derivative differ in their width (in the following, we will refer to the thinnest rows formed by one derivative as *mono*molecular rows and call the wider ones *multi*molecular rows). However, the borders of these lines always exhibit the same structure by which small rectangular cavities are formed (yellow rectangle in Figure 3.7b) in which one **P3** molecule is trapped. These cavities are interconnected by a small area (red rectangles in Figure 3.7b) in which the alkoxy chains of the nested **P3** molecules are situated. This structure gives rise to the rows consisting of **P3** molecules and thus they exhibit always the same width.

Two of the cavities formed by **ZnOEP** together with the trapped **P3** molecules are shown by the molecular models in 3.7b. Each cavity consists of six **ZnOEP** molecules which are partially being shared by adjacent cavities. The sides of the rectangular cavities have a mean length of (17.8 ± 0.8) Å and (13.2 ± 1.0) Å, which leads to a cavity size of (234.9 ± 15.8) Å^2. Estimating the area which is covered by **P3** is challenging. However, for the CuOEP molecule L. Ramoino was able to determine the occupied surface area on Cu(111) from LEED measurements to be 170 Å^2.[21] As the alkoxychains of **P3** are situated outside the cavities, we can approximate the area occupied by the **P3** molecule inside the cavities by the area which is covered by a CuOEP molecule on the Cu(111) surface. By doing so, we can conclude that the **P3** molecules fill the two-dimensional cavities to approximately $\frac{170}{235} \times 100\% \simeq 72\%$. From chemistry it is known that in solution binding molecules in a three-dimensional cavity of a molecular receptor is preferably done when the cavity is filled to 55%.[58] Larger values of up to 70% are expected for strong

intermolecular forces which further stabilize the formed complex. This is another interesting example, where the knowledge gained in three dimensions seems to be applicable to the two dimensional surfaces.

As the interaction of a **ZnOEP** molecule with a **P3** molecule is preferred over an interaction between two **ZnOEP** molecules, as shown above, the sole arrangement in *mono*molecular rows should be preferred over the formation of *multi*molecular rows which occurs due to the excess of **ZnOEP** molecules. In the following we will hence only discuss the interactions between the **ZnOEP** molecules with a **P3** molecules inside the cavities. The included molecular models in Figure 3.7b help in understanding these interactions. First, the cyano groups of the **P3** molecule can most probably interact via weak hydrogen bonds with the ethyl chains of adjacent **ZnOEP** molecules. Second, the alkoxy chains of the **P3** molecule are situated inside the small area which connects two adjacent cavities. Here, they are still mobile, as streaks in the STM images prove, but can also not only interact via van der Waals interactions with the alkoxy chains of the **P3** molecules in the adjacent cavities but also with the ethyl chains of adjacent **ZnOEP** molecules. Thus, for the **ZnOEP** molecules the preferred interaction with the alkoxy chains of **P3** is maximized. Interestingly, the alkoxy chains of **P3** are not completely immobilized which indicates that the van-der-Waals interactions are not strong enough for the alkoxy chains to completely condensate, but that they are nevertheless sufficient to direct the molecular self-assembly into the characteristic row pattern.

The existence of the mixed network demonstrates the importance of the entropy compensation mechanism for self-assembled networks. In the experiment presented in section 3.3.1 two very similar molecules which both contain the polar 4-cyanophenyl moiety formed separated phases. For the co-adsorption of **P3** and **ZnOEP** which both contain apolar alkyl chains, the structural arrangement into a mixed network is energetically more profitable, although the antiparallel dipole-dipole interactions exploited in the first experiment are stronger than van-der-Waals interactions.[59] Notably, these dipole-dipole interactions which in section 3.1 lead to the chains of **P3** at the same coverage are not found inside the mixed network. This shows nicely that the mechanism of enthalpy/entropy compensation can become so important that it can direct self-assembly more efficiently than the use of strongly interacting functional groups.

It is very interesting to compare the behavior of the intermixed system to that of lipid molecules in aqueous solution[13]. Lipid molecules consist of

[13]Such systems are described in many textbooks about biology and biophysics, as for example in Ref.[41]

a polar head-group to which long apolar alkyl chains are attached. In aqueous solution and at low concentrations, these molecules are found separated inside the solution. Above a critical concentration, however, the lipids form micelles, in which the apolar alkyl chains are separated from the solution inside the micelles by walls consisting of the polar head-groups. This decreases the entropy of the lipids, which is compensated by an increase of the entropy of the aqueous solution by a reordering of the water molecules. In the case of the **P3-ZnOEP** system, the **P3** molecules can be regarded as the solvent while the **ZnOEP** molecules resemble the dissolved molecules. Below a critical dissolvent concentration, the **ZnOEP** molecules do not interact with each other. However, as in the case of the lipids in the aqueous solution an interaction between the solvent and the dissolved molecules is observed. Above the critical dissolvent concentration the **ZnOEP** molecules form multimeres, as do the lipids. However, the loss of entropy in this system is compensated not by a decreased ordering of the solvent, but by increased van-der-Waals interactions. This difference in the two systems can be explained by the fact that the solvent in the lipid-water system, the water, does not have flexible substituents. Nevertheless, this comparison shows nicely the strong interlink between biophysics and surface physics.

Chapter 4

Conclusions and Outlook

The porphyrin molecule has proven to be a very versatile building block for self-assembly. Its rectangular core structure allows for the substitution of up to eight different side-groups. Depending on the choice of these groups, the resulting self-assembled structures can be either one-dimensional straight chains,[38] multimers,[60] or two-dimensional networks. The latter can be altered between either close-packed rectangular assemblies[23] or porous hexagonal ones.[61]

In this thesis, the focus lay on porphyrin derivatives with different alkylic substituents. In the first part of the results (section 3.1) we took advantage of the concept of synthons which is well known from supramolecular chemistry: We combined the well-known tetraphenyl porphyrin core with both the well-studied cyano synthon and different alkoxy synthons with different steric demands and flexibilities. Thus, we combined a polar and a less polar synthon into one entity to make use of a mechanism similar to the hydrophobic effect that has been described before by Desiraju *et al.*[62] This effect leads to a separation of the polar and apolar groups. In the 3D crystal structure, the cyano group has been observed to form assemblies of different geometries, namely linear dimers and cyclic trimers. We have shown that on the surface, depending on the steric demand of the chosen alkoxyphenyl substituents, the assembly can be forced correspondingly either into a one- or two-dimensional phase. The observed one-dimensional wires, in contrast to the straight ones presented by Yokoyama *et al.*,[38] are flexible and can have branchings. The two-dimensional nanoporous networks are a result of a separation of the polar groups which are situated inside the network and the apolar groups which form the pores. One parameter of these networks, namely the pore-to-pore distance, was changed in a controlled way. This was attributed to (i) the different steric demand of the alkoxy chains and (ii) the balancing of the entropic losses of these substituents by van-der-Waals interactions.

In the second part of the results (section 3.2) it was shown that a nanoporous network as presented in the first part can be used as the basis for a fully self-assembled supramolecular device. The molecular building block of the device is very similar to the one used in the first part. However, the flexible alkoxy chains are exchanged by bulky *tert*-butyl groups. As these groups which form the rim of a pore, are rigid and their conformational degree of freedom is mainly attributed to a rotation of the tertiary butyl groups around the phenyl-carbon bond, also the rim itself is, in contrast to the pores in the networks presented in the first part, rigid and thus well-defined. This leads to the possibility of nesting porphyrin guest molecules on top of the pores, presumably due to an interaction between the *tert*-butyl groups of the nested molecules and those of the molecules inside the network. This arrangement is therefore the result of a delicate relation between the pore diameter and the size of the nested guest molecules. Because of the symmetry of the system, the nested molecules are found in three distinguishable positions. By thermal activation or interactions with the tip, they can hop between these positions without disrupting the entity or hopping to a neighboring pore. The activation energy of such a hopping event was estimated to be 0.24 eV.

The investigated supramolecular multi-position device proves that by molecular self-assembly complicated structures mimicking macroscopic functional devices can be formed. However, the presented device has still some draw-backs, as for example the low temperature of operation. These problems and some possible solutions leading to future experiments have been presented and discussed.

In the last part of the results (section 3.3) the influence of the entropy on bimolecular systems has been investigated. Here it was shown, that different side-groups with different flexibilities can be utilized to steer the intermixing behavior of the molecular compounds. Two different systems were presented, which demonstrated how the mechanism of entropy compensation can be exploited to obtain either separated phases of the different molecular species, or a mixed network consisting of both molecular compounds.

The experiments and results presented in this thesis have greatly improved the knowledge of self-assembly processes on metal surfaces. They are the result of an intensive cooperation with chemists of the group of François Diederich at the ETH Zürich. This cooperation which has proven to be very fruitful and stimulating, made it possible to manage the sometimes difficult transfer from principles developed by chemists in the 3D bulk or in solution into the field of surface science. Based on this, the thesis at hand will be the basis for a number of future ideas and experiments which are currently being developed. Specifically, we want to investigate the interaction of the three different nanoporous networks presented in section 3.1 with different

molecules. As the pores of these networks consist of alkoxy chains of different size we are expecting them to exhibit different interactions with guest molecules. Furthermore, we are planning to use the one-dimensional chains observed in the same section as a "real" *Nanolab*. As the chains divide the metal surface into areas with different sizes, we want to trap single molecules inside these compartments to study their phase behavior depending on the temperature and the compartment size.

Appendix A

Supporting Information for Publication A

In the following, a shortened version of the supporting information as send to *Small* is presented.

(...)

3. Controlled switching between imaging modes

As stated in the main text, two characteristically different imaging modes were observed, in which either the π-system gives a strong signal (mode 1), or all parts of the molecule are equally visible (mode 2). The mode of imaging does not change with the applied voltage. However, by giving small voltage pulses of around 3.5 V, one can sometimes switch between the modes in a controlled way, as shown in Figure S-3. Here, also a third mode can be seen (which was not observed very often), in which the alkoxy chains are accentuated (denoted as mode 3) and a mixture between modes 2 and 3. Therefore, we think that the different imaging modes can be attributed to different tip conditions. Probably the tip apex is changed due to a picking up or a release of organic parts.

4. Alignment of the molecules within the chains with respect to the copper substrate

Figure S-4a shows an STM image of the chains of **3** on a Cu(111) surface. Both atomic resolution of the substrate and molecular resolution of the chains were obtained simultaneously. Interestingly, not all parts of the bare metal substrate are atomically resolved. This effect can be related to an individual molecule, which is trapped underneath the tip apex and dragged along with the scanning tip over the substrate before it is stripped off at the next

molecular chain.[3]

From such an image, we were able to determine the alignment of the molecules with respect to the substrate. We marked for each molecule the position of its characteristic dark line, which is caused by the two downwards tilted pyrrole rings of the porhpyrin core (see main text; green lines in Figure S-4a). In total, three different directions were found, whereas always two of them include an angle of approximately 120°.

The derivative of the STM image clearly shows the three main directions of the Cu(111) substrate (Figure S-4b). Next, the topographic STM image was superimposed with the derivative of that image (Figure S-4c). By this, the three molecular directions can be compared with the substrate directions (green and black cross in Figure S-4c). One has to keep in mind that in STM images drift effects are reflected in the slow scanning direction (here the vertical direction) much more than in the fast one (horizontal direction). The directions of the substrate can be determined with a higher precision than the directions of the dark lines, because of the small dimensions of an individual molecule. Nevertheless, the result shows that, within an uncertainty of 7 degrees, the characteristic dark lines follow the substrate directions.

The angle between the dark line, reflecting a diagonal through the porphyrin core, and the direction along the cyanophenyl group amounts to 135 degrees (anticlockwise). As the angle between the substrate directions is 120 degrees, straight sections within the molecular chains are tilted by an angle of (15 ± 7) degrees against the atomic directions.

5. Density dependent images of the molecular chains hinting on the formation of the networks

Figure S-5 shows STM images of the molecular chains whereas the coverage increases from from image (a) to (d). At low coverage, the chains have nearly no branches. With increasing coverage, also the number of branches increase. At very high coverages (about 0.8 ML, Figure S-5d), the formation of single pores can be observed. Hence, the transition from the chainlike arrangement to the networks **2** and **3** is caused by the decreased degree of freedom for each molecule within the first layer. Furthermore, the growth of the networks start with a single pore.

6. Schemes and Figures

(...)

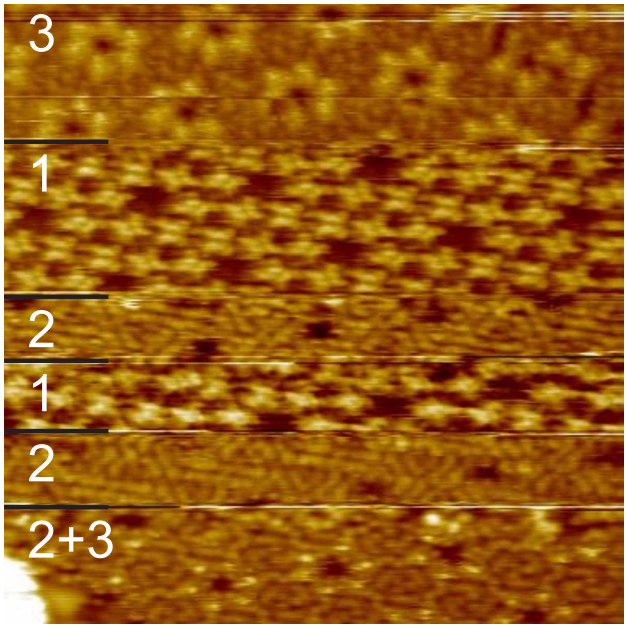

Figure A.1: (Figure S-3) STM image (25×25 nm^2; $U_{\mathrm{gap}} = -1.4$ V, $I_{\mathrm{tunnel}} = 20$ pA) of molecule **2** on Cu(111) at a coverage above 0.8 ML. The image shows that switching between the characteristical imaging modes can be obtained by applying voltage pulses (1: π-imaging mode, 2: all parts of the molecules give equal contrast, 3: the mobile alkoxy chains give the dominant signal).

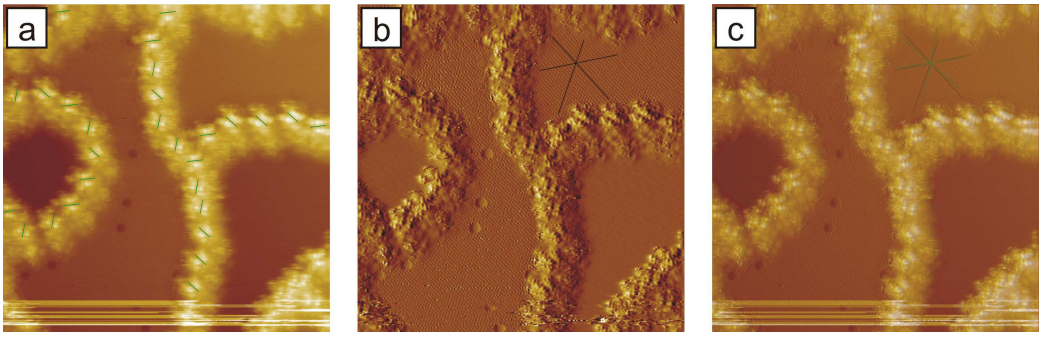

Figure A.2: (Figure S-4) a) STM image (25×25 nm^2; $U_{\mathrm{gap}} = +0.9$ V, $I_{\mathrm{tunnel}} = 10$ pA) of molecule **2** on Cu(111) at a coverage of about 0.2 ML. Both atomic resolution of the substrate and molecular resolution of the chains is obtained. The green lines emphasize the direction of the characteristic dark line in each molecule. b) In the derivative of the STM image the atomic resolution is more accentuated and thus, the three main directions (indicated by the black lines) can be easily identified. c) By overlaying the STM image with its derivative we can directly compare the directions of the characteristic dark line (green cross) with the atomic directions (black cross).

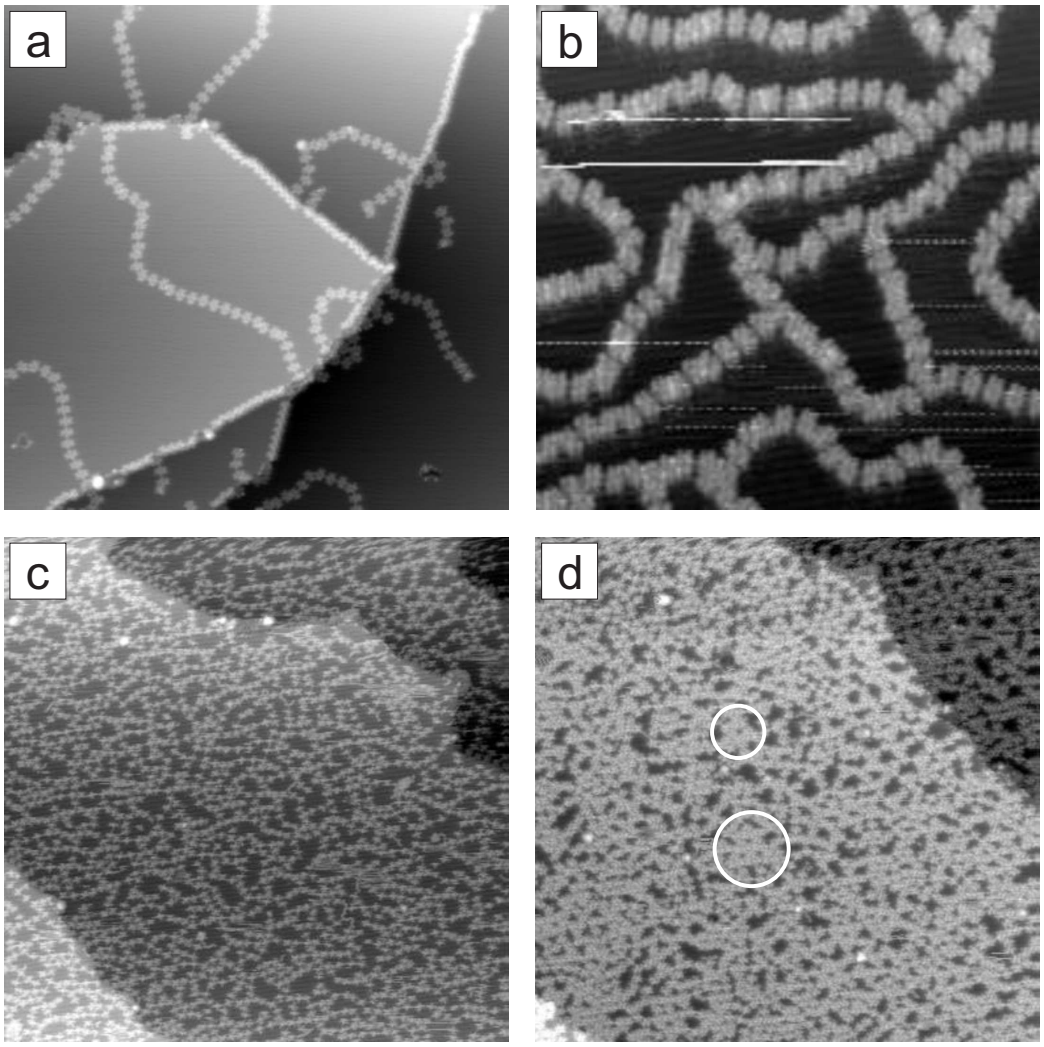

Figure A.3: (Figure S-5) STM images of the molecular chains of **2** with increasing coverages. a) Approx. 0.1 ML. No branching is observed (100×100 nm^2; $U_{\mathrm{gap}} = -1.5$ V, $I_{\mathrm{tunnel}} = 20$ pA). b) Approx. 0.3 ML (50×50 nm^2; $U_{\mathrm{gap}} = -1.4$ V, $I_{\mathrm{tunnel}} = 10$ pA) c) Approx. 0.7 ML. With increasing coverage also the number of branches increases (100×100 nm^2; $U_{\mathrm{gap}} = -1.5$ V, $I_{\mathrm{tunnel}} = 20$ pA). d) Approx. 0.8 ML. Single pores are formed which are marked by white circles (100×100 nm^2; $U_{\mathrm{gap}} = -1.5$ V, $I_{\mathrm{tunnel}} = 20$ pA).

7. References

(...)

[3] M. Böhringer, W.-D. Schneider, R. Berndt, K. Glöckler, M. Sokolowski, E. Umbach, *Phys. Rev. B* **1998**, *57*, 4081-4087.

Appendix B

Supporting Information for Publication B

Supporting Information

69451 Weinheim, Germany

A Supramolecular Multi-Position Rotary Device**

Nikolai Wintjes, Davide Bonifazi, Fuyong Cheng, Andreas Kiebele, Meike Stöhr, Thomas Jung*, Hannes Spillmann*, and François Diederich*

Details for nested guest molecules

As described in the main text, at a temperature of 77 K the guest molecules appear into the STM images as a rectangular structure with bright lobes at the edges which belong to the four *tert*-butyl residues contained in the 3,5-di(*tert*-butyl)phenyl substituents. In vacuum, both 3,5-di(*tert*-butyl)phenyl substituents are for steric / energetic reasons rotated by 60-90° against the central tetrapyrrolic core. Nevertheless, it is known that for porphyrins on metal surfaces this angle can be remarkably reduced due to molecule-surface interactions.[1] Therefore in the STM images four seperated lobes can be observed, which belong to one *tert*-butyl residue each.

The height of the guest molecules above the sample surface can only be roughly estimated. It depends on the dihedral angle of the 3,5-di(*tert*-butyl)phenyl substituents and the interaction with the surface and the six pore molecules. If all these interactions are ignored for an estimate, and we also assume that the nested molecule's down pointing part of one *tert*-butyl residue touches the directly underlying pore

molecule's up pointing part of this residue, the overall height corresponds to 1.5 times the effective height of one 3,5-di(*tert*-butyl)phenyl substituent. This estimation provides rather an upper limit, because, as illustrated in the three dimensional schematic representation in Movie 3, the 3,5-di(*tert*-butyl)phenyl substituents of the guest molecule can also lie in a way, that the down pointing part of one substituent lies over the down pointing part of one of the pore molecule's substituent. This leads to a lowered overall height of rather 1-1.1 times the effective height of the 3,5-di(*tert*-butyl)phenyl substituents. As described in the main text it is reasonable to assume a value of about 20° for the dihedral angle. Therefore the effective height of these groups is 5.4 Å and the guest molecule's height above the sample surface is 8.1 Å, using the estimations mentioned above (Figure 1). This means that even for this maximum value the guest molecule can still interact with the metal surface. This interaction leads to a bending of the molecule, explaining the observed reduction in the lobe distances of the guest molecules compared to the network molecules. Nevertheless, such a bending is only possible if the central tetrapyrrolic core is aligned parallel to the surface. This result is also supported by the fact, that the pore diameter is only 18 Å, but the distance from one 4-cyanophenyl group to the other is 21.6 Å. Therefore it is reasonable to assume a

parallel alignment of the central tetrapyrrolic core in respect to the underlying surface.

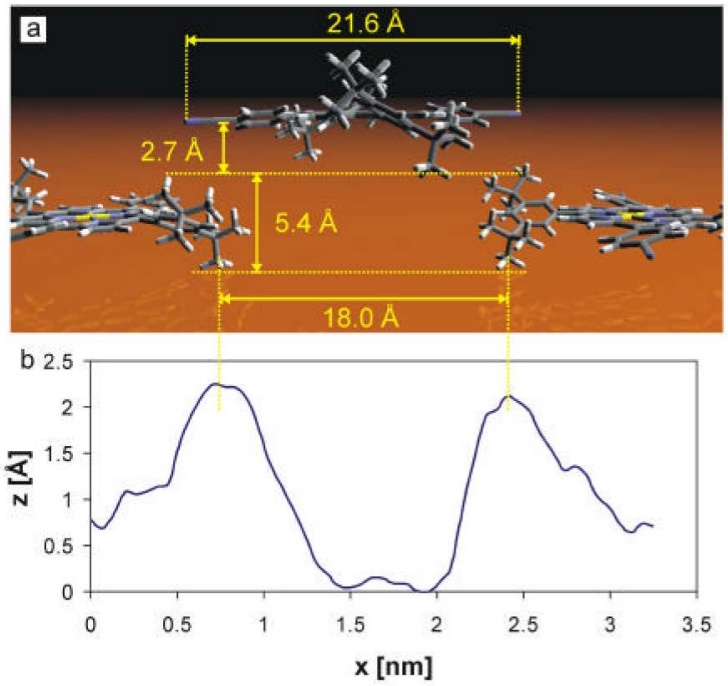

Figure 1 (SI). a) Three dimensional schematic representation of one pore with guest molecule. For reasons of clarity only three molecules are drawn and the expected bending of the guest molecule is not shown (for a more detailed view see Movie 3). The central tetrapyrrolic cores are aligned parallel to the underlying surface. The height of the pores depends on the rotational angle of the 3,5-di(*tert*-butyl)phenyl substituents, which we assume to be about 20° as described in the main text, and on the interaction with the metal surface. The given values belong to the height of the 3,5-di(*tert*-butyl)phenyl substituents (taken from vacuum) at a

dihedral angle of 20°. As the interaction with the Cu(111) surface is known to be strongly attractive, the realistic values will be rather smaller. b) Line cut across the STM data at the site of an unoccupied pore without nested guest molecule.

Movie 1. Time-lapsed STM imaging sequence (6 frames, real time difference between each frame is 148 s) showing the thermally induced rotation of rotary switches at 112 K. Single switching events can be resolved by the STM.

Movie 2. Time-lapsed STM imaging sequence (10 frames, real time difference between each frame is 148 s) showing the thermally induced rotation of rotary switches at 114 K. Because of the slow imaging speed of the STM compared to the rotational speed of the rotary switch at that temperature a single switching event can hardly be resolved. Therefore the rotors appear fuzzy.

Movie 3. Three dimensional schematic representation of a single pore with a nested guest molecule.

[1] T. A. Jung, R. R. Schlittler, J. K. Gimzewski, *Nature* **1997**, *386*, 696-698.

Bibliography

[1] G. Binnig and H. Rohrer, *Scanning tunneling microscopy*, Helvetica Physica Acta **55**, 726–735 (1982).

[2] G. Binnig, H. Rohrer, C. Gerber, and E. Weibel, *Tunneling Through A Controllable Vacuum Gap*, Appl. Phys. Lett. **40**, 178–180 (1982).

[3] F. J. Giessibl, S. Hembacher, H. Bielefeldt, and J. Mannhart, *Subatomic features on the silicon (111)-(7x7) surface observed by atomic force microscopy*, Science **289**, 422–425 (2000).

[4] Wolfgang Nolting, *Grundkurs Theoretische Physik 5/1*, Springer Verlag (2004).

[5] J. Bardeen, *Tunnelling From A Many-Particle Point Of View*, Phys. Rev. Lett. **6**, 57–59 (1961).

[6] C. J. Chen, *Introduction to Scanning Tunneling Microscopy*, Oxford University Press, New York (1993).

[7] N. D. Lang, *Spectroscopy Of Single Atoms In The Scanning Tunneling Microscope*, Phys. Rev. B **34**, 5947–5950 (1986).

[8] V. A. Ukraintsev, *Data evaluation technique for electron-tunneling spectroscopy*, Phys. Rev. B **53**, 11176–11185 (1996).

[9] J. Tersoff and D. R. Hamann, *Theory And Application For The Scanning Tunneling Microscope*, Phys. Rev. Lett. **50**, 1998–2001 (1983).

[10] J. Tersoff and D. R. Hamann, *Theory of the scanning tunneling microscope*, Phys. Rev. B **31**, 805–813 (1985).

[11] R. Wiesendanger and H.-J. Güntherodt, *Scanning Tunneling Microscopy III*, Springer Verlag, Berlin Heidelberg, 2nd ed. (1996).

[12] C. J. Chen, *Origin Of Atomic Resolution On Metal-Surfaces In Scanning Tunneling Microscopy*, Phys. Rev. Lett. **65**, 448–451 (1990).

[13] C. J. Chen, *Microscopic View Of Scanning Tunneling Microscopy*, J. Vac. Sci. Technol. A **9**, 44–50 (1991).

[14] D. Drakova, *Theoretical modelling of scanning tunnelling microscopy, scanning tunnelling spectroscopy and atomic force microscopy*, Rep. Prog. Phys. **64**, 205–290 (2001).

[15] A. M. Bar, R. Miranda, J. Alaman, N. Garcia, G. Binnig, H. Rohrer, C. Gerber, and J. L. Carrascosa, *Determination Of Surface-Topography Of Biological Specimens At High-Resolution By Scanning Tunnelling Microscopy*, Nature **315**, 253–254 (1985).

[16] J. K. Gimzewski, E. Stoll, and R. R. Schlittler, *Scanning Tunneling Microscopy Of Individual Molecules Of Copper Phthalocyanine Adsorbed On Polycrystalline Silver Surfaces*, Surf. Sci. **181**, 267–277 (1987).

[17] B. I. Lundqvist, O. Gunnarsson, H. Hjelmberg, and J. K. Nørskov, *Theoretical Description Of Molecule-Metal Interaction And Surface-Reactions*, Surf. Sci. **89**, 196–225 (1979).

[18] P. Sautet, *Images of adsorbates with the scanning tunneling microscope: Theoretical approaches to the contrast mechanism*, Chem. Rev. **97**, 1097–1116 (1997).

[19] R. Berndt, J. K. Gimzewski, and R. R. Schlittler, *Bias-dependent STM images of oxygen-induced structures on Ti(0001) facets*, Surf. Sci. **310**, 85–88 (1994).

[20] M. L. Bocquet and P. Sautet, *STM and chemistry: a qualitative molecular orbital understanding of the image of CO on a Pt surface*, Surf. Sci. **360**, 128–136 (1996).

[21] L. Ramoino, *Adsorption and Self-Organization of CuOEP on Heterogeneous Surfaces: Tuning the Molecule-Substrate Interaction*, Thesis (2005).

[22] J. Kröger, H. Jensen, R. Berndt, R. Rurali, and N. Lorente, *Molecular orbital shift of perylenetetracarboxylic-dianhydride on gold*, Chem. Phys. Lett. **438**, 249–253 (2007).

[23] T. A. Jung, R. R. Schlittler, and J. K. Gimzewski, *Conformational identification of individual adsorbed molecules with the STM*, Nature **386**, 696–698 (1997).

[24] J. K. Gimzewski, C. Joachim, R. R. Schlittler, V. Langlais, H. Tang, and I. Johannsen, *Rotation of a single molecule within a supramolecular bearing*, Science **281**, 531–533 (1998).

[25] F. Moresco, G. Meyer, K. H. Rieder, H. Ping, H. Tang, and C. Joachim, *TBPP molecules on copper surfaces: a low temperature scanning tunneling microscope investigation*, Surf. Sci. **499**, 94–102 (2002).

[26] J. K. Gimzewski, T. A. Jung, M. T. Cuberes, and R. R. Schlittler, *Scanning tunneling microscopy of individual molecules: beyond imaging*, Surf. Sci. **386**, 101–114 (1997).

[27] J. V. Barth, H. Brune, G. Ertl, and R. J. Behm, *Scanning Tunneling Microscopy Observations On The Reconstructed Au(111) Surface - Atomic-Structure, Long-Range Superstructure, Rotational Domains, And Surface-Defects*, Phys. Rev. B **42**, 9307–9318 (1990).

[28] F. Schreiber, *Organic molecular beam deposition: Growth studies beyond the first monolayer*, Phys. Stat. Sol. (a) **201**, 1037–1054 (2004).

[29] B. Hammer and J. K. Nørskov, *Why Gold Is The Noblest Of All The Metals*, Nature **376**, 238–240 (1995).

[30] T. Zambelli, Y. Boutayeb, F. Gayral, J. Lagoute, N. K. Girdhar, A. Gourdon, and S. Gauthier, *Deposition of Large Organic Molecules in Ultra-High Vacuum: A Comparison between Thermal Sublimation and Pulse-Injection*, Int. J. Nanoscience **3**, 331–341 (2004).

[31] T. Yamada, H. Shinohara, G. Maofa, S. Mashiko, and K. Kimura, *A molecular-beam apparatus with a spray-jet technique for studying neutral non-volatile molecules*, Chem. Phys. Lett. **370**, 132–138 (2003).

[32] J. C. Swarbrick, J. Ben Taylor, and J. N. O'Shea, *Electrospray deposition in vacuum*, Appl. Surf. Sci. **252**, 5622–5626 (2006).

[33] L. R. Milgrom, *The colours of life: an introduction to the chemistry of porphyrins and related compounds*, Oxford University Press (1997).

[34] M. B. Crute, *The crystal structure of nickel etioporphyrin-II*, Acta Cryst. **12**, 24–28 (1959).

[35] R. A. Collins and K. A. Mohammed, *Gas Sensitivity Of Some Metal Phthalocyanines*, J. Phys. D: Appl. Phys. **21**, 154–161 (1988).

[36] T. Nojiri, M. M. Alam, H. Konami, A. Watanabe, and O. Ito, *Photoinduced electron transfer from phthalocyanines to fullerenes (C-60 and C-70)*, J. Phys. Chem. A **101**, 7943–7947 (1997).

[37] H. Imahori and S. Fukuzumi, *Porphyrin- and fullerene-based molecular photovoltaic devices*, Adv. Funct. Mater. **14**, 525–536 (2004).

[38] T. Yokoyama, S. Yokoyama, T. Kamikado, Y. Okuno, and S. Mashiko, *Selective assembly on a surface of supramolecular aggregates with controlled size and shape*, Nature **413**, 619–621 (2001).

[39] S. Buchholz and J. P. Rabe, *Conformation, Packing, Defects, And Molecular-Dynamics In Monolayers Of Dialkyl-Substituted Benzenes*, J. Vac. Sci. Technol. B **9**, 1126–1128 (1991).

[40] G. M. Whitesides, J. P. Mathias, and C. T. Seto, *Molecular Self-Assembly And Nanochemistry - A Chemical Strategy For The Synthesis Of Nanostructures*, Science **254**, 1312–1319 (1991).

[41] G. Adam, P. Läuger, and G. Stark, *Physikalische Chemie und Biophysik*, Springer Verlag (1995).

[42] H. Tang, M. T. Cuberes, C. Joachim, and J. K. Gimzewski, *Fundamental considerations in the manipulation of a single C-60 molecule on a surface with an STM*, Surf. Sci. **386**, 115–123 (1997).

[43] F. Moresco, *Manipulation of large molecules by low-temperature STM: model systems for molecular electronics*, Physics Reports-Review Section Of Physics Letters **399**, 175–225 (2004).

[44] D. M. Eigler, C. P. Lutz, and W. E. Rudge, *An Atomic Switch Realized With The Scanning Tunneling Microscope*, Nature **352**, 600–603 (1991).

[45] D. Bonifazi, H. Spillmann, A. Kiebele, M. de Wild, P. Seiler, F. Y. Cheng, H. J. Güntherodt, T. Jung, and F. Diederich, *Supramolecular patterned surfaces driven by cooperative assembly of C-60 and porphyrins on metal substrates*, Angew. Chem. Int. Ed. **43**, 4759–4763 (2004).

[46] M. Stöhr, M. Wahl, H. Spillmann, L. H. Gade, and T. A. Jung, *Lateral Manipulation for the Positioning of Molecular Guests within the Confinements of a Highly Stable Self-Assembled Organic Surface Network*, Small **3**, 1336 (2007).

[47] L. S. Pinheiro and M. L. A. Temperini, *Coadsorption of 2-mercaptopyrimidine and 1,10 '-phenanthroline on Au(111) as seen by STM*, Surf. Sci. **441**, 53–64 (1999).

[48] M. de Wild, S. Berner, H. Suzuki, H. Yanagi, D. Schlettwein, S. Ivan, A. Baratoff, H. J. Guentherodt, and T. A. Jung, *A novel route to molecular self-assembly: Self-intermixed monolayer phases*, ChemPhysChem **3**, 881–885 (2002).

[49] C. Bobisch, T. Wagner, A. Bannani, and R. Möller, *Ordered binary monolayer composed of two organic molecules: Copper-phthalocyanine and 3,4,9,10-perylene-tetra-carboxylic-dianhydride on Cu(111)*, J. Chem. Phys. **119**, 9804–9808 (2003).

[50] J. A. Theobald, N. S. Oxtoby, M. A. Phillips, N. R. Champness, and P. H. Beton, *Controlling molecular deposition and layer structure with supramolecular surface assemblies*, Nature **424**, 1029–1031 (2003).

[51] L. Scudiero, K. W. Hipps, and D. E. Barlow, *A self-organized two-dimensional bimolecular structure*, J. Phys. Chem. B **107**, 2903–2909 (2003).

[52] M. E. Cañas Ventura, W. Xiao, D. Wasserfallen, K. Müllen, H. Brune, J. V. Barth, and R. Fasel, *Self-assembly of periodic bicomponent wires and ribbons*, Angew. Chem. Int. Ed. **46**, 1814–1818 (2007).

[53] K. Tahara, S. Furukawa, H. Uji-I, T. Uchino, T. Ichikawa, J. Zhang, W. Mamdouh, M. Sonoda, F. C. De Schryver, S. De Feyter, and Y. Tobe, *Two-dimensional porous molecular networks of dehydrobenzo[12]annulene derivatives via alkyl chain interdigitation*, J. Am. Chem. Soc. **128**, 16613–16625 (2006).

[54] S. Stepanow, M. Lingenfelder, A. Dmitriev, H. Spillmann, E. Delvigne, N. Lin, X. B. Deng, C. Z. Cai, J. V. Barth, and K. Kern, *Steering molecular organization and host-guest interactions using two-dimensional nanoporous coordination systems*, Nat. Mater. **3**, 229–233 (2004).

[55] A. Kiebele, D. Bonifazi, F. Y. Cheng, M. Stöhr, F. Diederich, T. Jung, and H. Spillmann, *Adsorption and dynamics of long-range interacting fullerenes in a flexible, two-dimensional, nanoporous porphyrin network*, ChemPhysChem **7**, 1462–1470 (2006).

[56] J. P. Sestelo and T. R. Kelly, *A prototype of a rationally designed chemically powered Brownian motor*, Appl. Phys. A **75**, 337–343 (2002).

[57] K. W. Hipps, X. Lu, X. D. Wang, and U. Mazur, *Metal d-orbital occupation-dependent images in the scanning: Tunneling microscopy of metal phthalocyanines*, J. Phys. Chem. **100**, 11207–11210 (1996).

[58] S. Mecozzi and J. Rebek, *The 55% solution: A formula for molecular recognition in the liquid state*, Chem. Eur. J. **4**, 1016–1022 (1998).

[59] J.W. Steed and J. L. Atwood, *Supramolecular Chemistry*, Wiley-VCH (2000).

[60] T. Yokoyama, T. Kamikado, S. Yokoyama, and S. Mashiko, *Conformation selective assembly of carboxyphenyl substituted porphyrins on Au (111)*, J. Chem. Phys. **121**, 11993–11997 (2004).

[61] H. Spillmann, A. Kiebele, M. Stöhr, T. A. Jung, D. Bonifazi, F. Y. Cheng, and F. Diederich, *A two-dimensional porphyrin-based porous network featuring communicating cavities for the templated complexation of fullerenes*, Adv. Mater. **18**, 275–+ (2006).

[62] G. R. Desiraju, *Supramolecular Synthons In Crystal Engineering - A New Organic-Synthesis*, Angew. Chem. Int. Ed. **34**, 2311–2327 (1995).

Acknowledgements

I would like to thank the following people for their help in making this PhD project a success:

- Prof. Dr. Güntherodt and Dr. T. Jung for the opportunity to work in the *Nanolab*.
- PD Dr. H. Spillmann for being my supervisor who led me into the field of STM and for patient explanations.
- Dr. M. Stöhr, Dr. J. Lobo-Checa and M. Matena for helpful discussions and their support in writing this thesis.
- S. Schnell for sample preparations and assistance regarding technical and mechanical problems.
- The group of Prof. F. Diederich (especially J. Hornung, T. Voigt and L.-A. Fendt) for the synthesis of the chemical compounds and for invaluable scientific discussions.
- The secretaries of the University of Basel for their help with beaurocratical non-sense.
- The whole group of the *Nanolab* for patience while having lunch together.
- My friends and my family for their support.
- Prof. Ulrich Seydel, who taught me everything I know about biological systems and provided me with the opportunity to write my diploma work in his group, which proofed to be a valuable enrichment also of this thesis.

Publications and Conferences

Conference Participations

09.2007 **TNT**, San Sebastian, Spain. Oral presentation
Supramolecular Rotor-Stator Systems leading to a Multi-Position Rotary Device

07.2007 **ICN&T**, Stockholm, Sweden. Oral presentation
An Addressable Supramolecular Multi-Position Rotary Device

03.2007 **DPG**, Regensburg, Germany. Oral presentation
An Addressable Supramolecular Rotary Switch Featuring Distinguishable Positions Embedded In A Two-Dimensional Porphyrin-Based Porous Network

02.2007 **SPS**, Zürich, Switzerland. Oral presentation
An Addressable Supramolecular Rotary Switch Featuring Distinguishable Positions Embedded In A Two-Dimensional Porphyrin-Based Porous Network

09.2006 **ECOSS**, Paris, France. Oral presentation
Dynamics of long-range interacting C60 and C70 fullerenes hosted in a 2D-nanoporous porphyrin network

03.2006 **DPG**, Leipzig, Germany. Oral presentation
Two-dimensional Porphyrin-based Porous Network Featuring Communicating Cavities

01.2006 **SAOG**, Fribourg, Switzerland. Oral presentation
Two-dimensional Porphyrin-based Porous Network Featuring Communicating Cavities

Publications

2007 N. Wintjes, D. Bonifazi, F. Cheng, A. Kiebele, M. Stöhr, T. Jung, H. Spillmann, and F. Diederich, *A Supramolecular Multiposition Rotary Device*, Angew. Chem. **119**, 4167-4170 (2007); Angew. Chem. Int. Ed. **46**, 4089-4092 (2007).
DOI: 10.1002/ange.200700285

2007 N. Wintjes, J. Hornung, J. Lobo-Checa, T. Voigt, T. Samuely, C. Thilgen, M. Stöhr, F. Diederich and T. A. Jung, *Controlling Dimensionality and Periodicity of Supramolecular Assemblies on Surfaces by Rational Modifications of Alkoxy Substituents*, submitted to *Small*.

2007 T. Samuely, M. Stöhr, N. Wintjes, T. A. Jung, M. Haas, S.-X. Liu, S. Decurtins, *Phthalocyanine derivatives on noble metal surfaces*, in preparation for the *Journal of Physical Chemistry C*.

2007 N. Wintjes, J. Hornung, J. Lobo-Checa, M. Stöhr, T. Samuely, F. Diederich and T. A. Jung, *Tuning the interactions in bimolecular systems on surfaces*, in preparation.

Patents

2006 N. Wintjes, H. Spillmann, D. Bonifazi, A. Kiebele, F. Cheng, H.-J. Güntherodt, T. Jung and F. Diederich, *A molecular three way rotary switch also able to store information hosted by a molecular matrix*, US patent 60/831,111, filed 14. 7. 2006.

Articles in the Media about the Rotary Device

2007 *Ein Molekül wird zum Nanoschalter*
Horizonte, **74**, p.6 (2007)

2007 *Millionen Schalter im Netzwerk*
CHemie Plus **7-8/07**, p.8 (2007)

2007 *Ein Nanoschalter aus Molekülen*
NZZ (Neue Züricher Zeitung), 6. Juni 2007

2007 *Millionen Schalter im Netzwerk*
Swiss Nanoscience Institute, 25. Mai 2007

Curriculum Vitae

Persönliche Daten

Name:	Wintjes
Vorname:	Nikolai Jens
Geburtsdatum:	12.12.1977
Geburtsort:	Marl, NRW, Deutschland
Staatsangehörigkeit:	deutsch
Familienstand:	ledig
Eltern:	Marianne und Klaus-Peter Wintjes

Ausbildung

Doktorat:	seit Mai 2005: Doktorrand am Institut für Physik, Universität Basel 2007: Gewinner des *Best Nano Image Award 2007* des NCCR Nanoscale Science
Diplomarbeit:	*Optimierung von Meßparametern für Elastizitätsmessungen an Zellen mit dem Rasterkraftmikoskop* Bewertung: sehr gut, ausgezeichnet mit dem Diplompreis 2004 des Vereins zur Erforschung infektiologischer und allergologischer Prozesse e.V.
Hochschule:	Oktober 1998 - Dezember 2004: Studium im Fach Physik an der Christian-Albrechts-Universität zu Kiel Erlangen des Diploms im Dezember 2004 (Note: sehr gut mit Auszeichnung)
Gymnasium:	August 1988 - Mai 1997: Gymnasium Im Loekamp (Marl) Erlangen der Hochschulreife im Mai 1997 (Note: 1,5)
Grundschule:	August 1984 - Juli 1988: Max-Reger-Grundschule (Marl)

Sonstiges

08.1999 - 09.2003:	Arbeit im Druck-Zentrum des Print & Copy Paradies, Kiel
08.1997 - 09.1998:	Zivildienst an der Tagesschule für geistig behinderte Kinder “Glück-Auf” (Marl)
09.1993:	Sprachkurs am St. Hildas College in Oxford, England